Optics & Laser Technology 143 (2021) 107284

Contents lists available at ScienceDirect

Optics and Laser Technology

journal homepage: www.elsevier.com/locate/optlastec

Full length article

Improvements of hybrid laser arc welding for shipbuilding T-joints with 2F position of 8 mm thick steel

C. Churiaque [a], J.M. Sánchez-Amaya [a,*], Ö. Üstündağ [b], M. Porrua-Lara [c], A. Gumenyuk [b,d], M. Rethmeier [b,d,e]

[a] Department of Materials Science and Metallurgical Engineering and Inorganic Chemistry, School of Engineering, University of Cádiz, Spain
[b] Bundesanstalt für Materialforschung und -prüfung (BAM), Germany
[c] Navantia S.A., S.M.E., Astillero Bahía de Cádiz, Spain
[d] Fraunhofer Institute for Production Systems and Design Technology, Germany
[e] Technische Universität Berlin, Germany

ARTICLE INFO

Keywords:
Hybrid laser arc welding
Naval steel
T-joints
Process parameters
Shipbuilding industry

ABSTRACT

One of the main concerns in the early stages of manufacturing flat units of shipbuilding is to ensure the quality of the joints throughout the structure. The flat units are constituted by butt welded flat plates, on which longitudinal T-welded reinforcements are placed to rigidize the structure. Among the different welding technologies, Hybrid Laser Arc Welding (HLAW) is becoming a mature process, profitable and highly productive. In addition, more innovative welding equipment are being developed nowadays, offering greater work flexibility, and raising expectations of achieving better quality, and economic viability. Another key point of HLAW to keep in mind is that structural distortions are reduced, resulting in decreasing the cost and time of straightening work.

In the present contribution, the influence of HLAW parameters on the quality of fillet joints of naval steel has been analysed. Experimental HLAW tests were performed with a high power disk laser to join EH36 naval steel plates, with a T configuration. The influence of different processing parameters has been analysed, as the laser power, welding speed, wire feed rate and the configuration of the HLAW processes (including head angle and laser/arc leading process). In addition, FEM simulations were carried out in order to estimate residual stresses and distortion of welded part. The distortion values provided by FEM presented excellent agreement with the measured experimental results. To evaluate the welds, non destructive tests including X-ray tests, metallographic analysis of cross sections, and microhardness mapping tests were performed.

Full penetration 8 mm T welds were obtained for the first time at an industrially applicable 2F position with a reasonable HLAW head angle, in one single step without sealing root, and using zero gap square groove edge preparation. The present contribution presents welding rates up to 2.2 m/min for 2F T-joints of this steel thickness, a much higher processing velocity than previously reported for industrial applications.

1. Introduction

1.1. Industrial application of hybrid laser arc welding technology

Hybrid Laser Arc Welding (HLAW) technology is gaining significance among all applicable welding processes in the industry. Specifically, sheet metal processing in heavy industry is considered an excellent field of application for HLAW as it combines the advantages of both laser and electric arc welding processes [1]. In general, HLAW reduces the work of preparing the bead and facilitates the union between difficult to weld materials [2].

HLAW is an attractive joining method as a single pass welding technique for medium thickness plates. It uses high energy processes to achieve a high penetration depth and high welding speeds that offer a substantial increase in productivity. Mainly, studies have addressed the influence of welding speed, laser power and other basic parameters of the HLAW process, being the butt joint the most commonly analysed welding configuration, as reviewed by Churiaque et al. [2].

HLAW technology has been successfully applied to join a great variety of metallic alloys, including different grades of steel, aluminium,

* Corresponding author.
E-mail address: josemaria.sanchez@uca.es (J.M. Sánchez-Amaya).

https://doi.org/10.1016/j.optlastec.2021.107284
Received 15 September 2020; Received in revised form 6 May 2021; Accepted 25 May 2021
Available online 5 June 2021

copper, nickel, and titanium alloys. For example, applications of HLAW on high yield strength steels is undertaken by Gorka [3], in which 10 mm thickness S700MC steel plates (a high strength steel grade used in light weight steel constructions) were welded at T configuration. Although full penetration was not achieved, a weld depth of 8 mm was reported at laser leading configuration with a welding speed of 1.1 m/min, and edges prepared as square butt joint without gap. High strength pipeline steel X120 has been recently joined with HLAW technology by Üstündağ et al. [4], reporting many economic benefits, such as lower material consumption and a reduction in transport and manufacturing costs. Another interesting research work regarding the benefits of using HLAW technology to join hardly weldable metals has been reported by Ramkumar et al. [5], in which AISI 416 (a martensitic grade stainless steel highly employed by nuclear, chemical and petrochemical industries), was successfully welded. Joints free from hot solidification cracking were successfully obtained using laser leading HLAW, with a suitable filler metal (Ni-Cr-Mo rich austenitic filler metal). The mechanical tests performed confirmed that the strength of the welded joint was much higher than the base metal.

In addition to the technical benefits of HLAW, numerous researches confirm that this technology provides a series of synergic effects and economic advantages that make it a profitable welding process for its implementation in different manufacturing sectors demanding high quality welds of thick sheet metal parts, such as hydraulic, offshore, pneumatic, aeronautical, and railway industries [6]. Another interesting study for the railway industry was presented by Liu et al. [7], with the aim of optimizing the process parameters for the manufacturing of high-speed bogie for railway vehicles. The HLAW process was applied to obtain T-joints of 12 mm thickness S355 steel (common material used to manufacture railway bogies) without groove. Full penetration sound and stable welds were achieved on one-side welding.

In this context, the HLAW installation allows a wide variety of customized combinations of laser and electric arc, offering great flexibility not only in the materials to be processed but also in the application possibilities.

1.2. Application of HLAW to shipbuilding

As for shipbuilding industry, a dominant driving force behind the introduction of laser technology in welding processes is the reduction of distortion. Ning et al. [8] experienced that the distortion of the laser welded joint was approximately 21% of that of the conventional welded joint and resulted in a significant improvement about 3.75 times in production efficiency. Specifically, shipbuilding takes advantage of this virtue provided by the laser source together with the GMA source in the hybrid process, to apply HLAW to the construction of cruise ships and military vessels. A number of factors play a role in determining the effects of the reduction in thermal distortion generated by hybrid welding. A significant analysis and discussion on the subject was presented by Olschok [9], stating that HLAW leads to a reduction in post-welding corrective processes, such as straightening operations and rework tasks. Drawing on an extensive range of welding tests, the author set out that rework costs are estimated at around 15%-30% of total staff costs in new constructions.

Another aspect that affects the general manufacturing production rate of the shipyards is the increase in the welding speed when the HLAW technology is applied. Sanchez-Sotano et al. [10], demonstrated in a recent simulation study that a potential productivity increase of 33% can be obtained in terms of numbers of shipyard structures manufactured per year when conventional welding processes is replaced by HLAW.

In order to save as much welding time as possible and unproductive time, as well as to obtain high quality joints, both butt plate welding and longitudinal profiles welding of the flat panel line should be produced one by one using the HLAW process.

Currently, in most shipyards, longitudinal welding is performed on both sides using the GMA procedure. This results in a thermal distortion due to high energy input, and consequently an expensive and time-consuming straightening work. These panels must be welded connecting the deck plates and the longitudinal stiffeners. Longitudinal reinforcements are fastened to the liner with hydraulic punches, if possible without gaps, and then tightened. In this way, gaps of up to 1 mm can appear between stiffeners and deck plates (flat panels). Nowadays, the newest HLAW equipment offers the integration of several processes (dimensional control, machining and welding) in the same station, providing really tight machining tolerances in the preparation of edges that reduce the gap.

The high welding speed, the appropriate tolerance adjustment, the deep penetration and the high quality of reported joints, are relevant reasons to propose the implementation of HLAW technology for welding longitudinal reinforcements in flat structures manufacturing line for shipbuilding.

The HLAW process has been used in shipbuilding since the beginning of the century at the prefabrication of the first two production steps of the deck section, within the flat block workshop. The manufacture of flat panels is a crucial process for the whole ship production, since it can represent about 50% of the welding work necessary for its construction [9]. In this first stage the HLAW process is most applicable. Currently, HLAW is increasingly present in the shipbuilding industry due to its low heat input, high quality and fast productivity. It is worth mentioning that the main European shipyards have implemented HLAW technology, mainly for the construction of flat panels [11].

According to the shipbuilding sequence, in the hull assembly process, the skin plates are welded together to become a block which is approximately 20 m^2, and longitudinal and transverse webs are fitted and welded [12]. In this pre-assembly stage executed in the flat panel line, two main types of joints are carried out:

- Butt joints of flat plates. This is the first step within the flat panel line. Initially, this first stage requires a good edges preparation, which is done by machining the edges of the plates. The plates are fixed together and then welded with the welding equipment, forming large panels (20 m × 20 m).
- T joints between the flat plates and the longitudinal stiffeners. This second type of welding allows joining reinforcements that connect different elements of the ship structure. The longitudinal profiles can have dimensions of 20 m × 0.2 m and a separation between stiffeners under 600 mm. The reinforcements are mechanically fixed to the panel to weld them without turning the structure. The HLAW process is used changing the angle of welding to get full connection, which requires a different geometric arrangement than the one used for butt joints, in order to ensure a complete connection.

Some recent HLAW studies try to solve the formation of drops produced by the imbalanced forces that act in the keyhole and the surface of the melting pool when thick plates are welded in a single pass. Üstündag et al. [13] apply a magnetic support based on the generation of Lorentz Forces, avoiding the use of any physical backing. Tang et al. [14] focus their recent research on investigation of humping formation process, underlining the important balance of surface tension and molten pool gravity. Arc-leading configuration is reported to be more beneficial to supress humping than Laser-Leading, due to the higher electrical stability [14].

Current advances in computational calculation technologies and the development of simulation methods based on finite elements (FEM) allow the optimization of industrial forming processes. A novel research uses numerical simulations to reproduce the phenomena observed experimentally and to study the formation mechanism of the bulge Marangoni effect taking place inside the weld [15]. Farroki et al. [16] have also successfully developed a novel adaptive double-conical heat source for the finite element simulation of butt hybrid laser welding of high thickness steel. Interestingly, thermal cycles and heat distribution

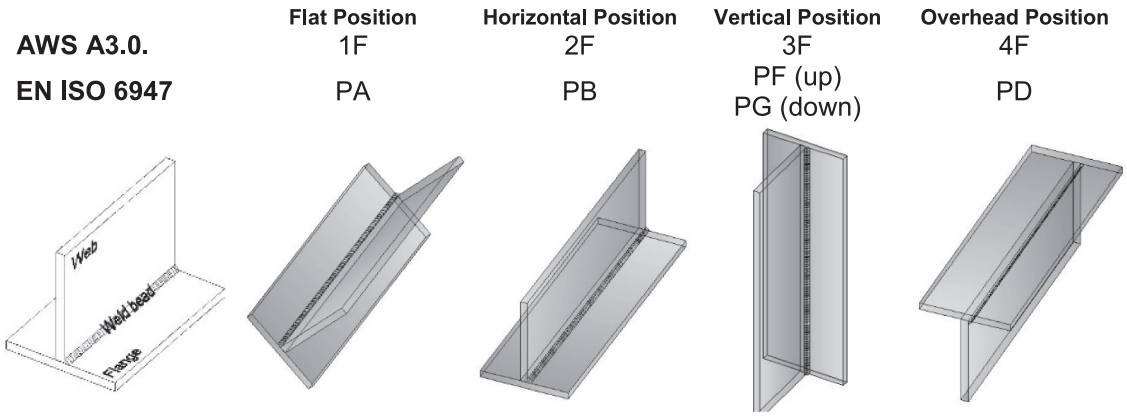

Fig. 1. Welding positions for fillet joints.

are reported to be significantly different in full and partial penetration welds, using the same welding heat input [16]. Simulation and experimental studies of fillet HLAW of aluminium alloy 6061 in the horizontal position are reported by Xu et al. [17]. Authors improved the keyhole stability and reduce the porosity formation by means of fitting the inclination heat source and enhancing the welding current. In [18], different welding sequences are studied in a stiffened panel on a semi-industrial scale. It could be appreciated that welding sequence plays an important role in the deformation of the structures. Less distortion was achieved by employing a change of direction in the mid-section of a reinforced panel in addition to alternating trajectories between two consecutive reinforcement welds. Bunaziv et al. [19] applied the numerical simulation model to predict the cooling rates in the joint and correlate these values with the hardness of the material and the evolution of the microstructure. The numerically estimated cooling rates for these joints presented a good fit with the experimental results, in which a lower cooling rate promoted wider fusion zone.

1.3. Application of HLAW to T-joints

Full penetration T-joint with fillet welding from one side is a demanding case by industry. The implementation of HLAW technology for the T-joint of longitudinal profiles on the lining would require the use of smaller hybrid heads adapted to the operating space, manipulated with robots or crane bridges with mobility in two horizontal and one vertical direction. In this sense, the use of robust hybrid heads normally used in the laboratory would not be possible in limited spaces such as the profile welding station of shipbuilding flat block workshop, as a consequence of the physical interference between the welding equipment head, stiffeners and deck plates. In fact, hybrid laboratory heads are more versatile, allowing the GMA torch to be decoupled from the laser source to adopt angle settings with greater degrees of freedom for different investigations. It is worth mentioning that hybrid heads for industrial application are in constant evolution and development. Nowadays, industrial systems offer interesting characteristics regarding their dimensions, which allow them to be adapted to a limited operating space, presenting a high degree of movement range.

Information on T-joint with HLAW technology is still limited, despite having an important niche in the naval sector. In addition, most T-joint welding studies have been carried out using CO_2 [20] and Nd:YAG [21] laser sources, which are currently being replaced by high power fiber or disk laser. Fiber and disk lasers provide high beam quality, generating better welding geometry together with a better total efficiency.

The effectiveness of HLAW technology for welding reinforcements has been demonstrated in several researches, bringing hopeful results for industrial application [20–24].

One of the key aspects that must be taken into account in the execution of T-joints is the welding position used, which is given depending on how the hybrid head is oriented with respect to the welded part. Welding positions are described in various normative documents, as EN ISO 6947: 2019 [25] and AWS A3.0: 2010 [26]. Fig. 1 shows images of welding positions according to the American Welding Society (AWS) and to the ISO standard.

One of the most commonly adopted configurations for researchers to weld T-joints is flat position (1F/PA). For example, Mazar Atabaki et al. [27], fixed the Flange plate establishing an inclination with respect to the horizontal plane at an angle of 35°- 45°. In a similar case developed by Liu et al. [7], plates were clamped to an angle adjuster positioned at 30° with respect to the surface. Unt et al. [28], showed that it is possible to obtain good quality full penetration welds with HLAW processes on 8 mm thick plates at 1F position. Their study focused on the effect of the initial sealing welding pass, run with defocused laser beam, on the quality of T-joint fillet welding. The quality of welds improves with this initial sealing welding pass, as the defects of the root side are minimised, such as irregular fusion, and lack of penetration, but the production slows down. Sound welds with good surface quality were also made in 10 mm thickness at the 1F position in [28], although full penetration was not obtained. One of the problems presented by the 1F fillet welding position is that it is not reproducible at industrial scale within the shipyard since flat panels are formed in 2F position.

Tsibulskiy et al. [24] followed a similar approach as that used in [28] to weld T-joints by HLAW with 1F position. Gaps between flange and web were fixed from 0.1 mm to 1 mm, working with an angle of incidence of the laser with respect to the flange of 5° [24]. This case revealed that a gap of 0.1 mm is optimal for welding T-joints.

It has also been reported by Bunaziv et al. that the presence of gap between welded plates increases deep penetration in the root zone, both in fillet [19] and butt [29] welds. This may be related to a more favourable melt flow, which allows the filler wire to be transported more effectively to the root because it requires less volume of base metal to be melted [19,29]. The authors indicate that the gap improves the entry of the laser beam into the joint and increases multiple reflections within it, causing greater absorption of the beam and more efficient fusion. It should be also noted that an increase in the gap has a negative effect on the deposition rate, and the wire feed rate must be increased when the gap is widened.

These geometrical arrangement parameters contribute significantly to the development of longitudinal welds to joint stiffeners to deck plates inside flat-block workshop of shipyard. However, keeping the air gap distance constant over the entire 20 m bead length would make the production process more complex and compromise costs and delivery times. It is also evident that the low angle configuration, 1F welding position and fitted gaps used in this approximation present some complexity to be implemented in shipyard workshops.

Edge preparation is also a key experimental parameter to be considered in hybrid welding of T-joints. Both Olschok [9] and Bunaziv

et al. [19] propose the realization of a small bevelling on the edge of the stiffener (web), maintaining an opening angle with the flange, which boosts the entry of the laser beam to the root. Complex edge preparation (bevel groove), such as chamfering, improve the HLAW process efficiency, but would also slow down production. In fact, the machining of plates with straight edges simplifies and speeds up the takt time of the flat panel lines of the shipyards, making it a most feasible option.

The amount and distribution of laser input energy, resulting from the power of the laser beam and the focal position, are also parameters that greatly influence root formation in HLAW process. A series of experimental tests is required in order to adjust the geometric configuration of the laser and arc power sources, and to obtain acceptable quality of the weld bead. The effect of laser power distribution is analysed by Unt et al. [22], where the different optical configurations and the fiber diameter (200, 300 and 600 μm) are investigated. The hybrid laser welding system equipped with 600 μm diameter fibers presented the best results regarding the quality of the joints. The welds had a broad root, which is crucial to achieve fusion at the back of the weld. Therefore, to avoid problems with beam positioning, the use of high laser powers with 600 μm fiber expands the process window for acceptable quality without the need for root sealing. The energy input distribution is therefore a key parameter to bear in mind, as it will influence the proper positioning of the hybrid head to obtain high welding quality.

In order to apply HLAW, a large number of parameters must be considered to achieve a stable welding process producing good quality joints. In order to predict the shape of the weld, it is essential to understand the phenomena that affect the formation of the weld bead. The weld width is of significant importance, since obtaining fusion in the whole plane of the joint is a challenge because HLAW provides narrow seams with limited tolerances. The influence of process parameters to obtain T-joints of B quality class is methodologically studied in [30]. The optimized experimental variables to weld low alloy steels S355 and AH36 in different thicknesses (6 mm, 8 mm and 10 mm) are reported. Full penetration was achieved for the 8 mm thick plates, maintaining a gap of 0.5 mm. Meanwhile, gapless welds achieved 75% penetration of the total thickness.

Most research studies agree that metallographic analyses of weld bead cross sections are essential to evaluate the weld quality and guarantee the HLAW process stability. Full penetration welds with a wine-cup shape are typical for HLAW. It is worth mentioning that, macro-sections corresponding to T-joints have an analogous shape to the wine-cup morphology for butt joints. Nevertheless, T-joints show the exception of adopting an inclination that depends on the fitted angle of the laser and arc sources to carry out the welds. This angle obviously influences the final morphology of the T weld.

An important theoretical issue that has dominated the field of application of HLAW has been the estimation of the structural strength of the bead. T weld is calculated from the thickness of the throat. These parameters are specified in the regulations of the classification societies as Bureau Veritas [31] or Lloyd's Register [32]. Proper adjustment of laser power and angle of incidence allows the root fusion, leading to an appropriate connection between flange and web. The throat dimensions are also influenced by the electric arc source [33]. External observation of most weld grooves predicts that they are within the limits of the thickness of the material being joined, but this appreciation by visual inspection makes it difficult to confirm the adequacy of the minimum design throat thickness. To verify both the dimensions and proportions of the throat, as well as to guarantee the full penetration and complete union of the pieces, it is necessary to make macrographic tests of a representative section of the bead, where weld imperfections as porosity, cracks, undercuts, or humps can be detected.

1.4. Scope and objectives

The research presented here focuses on the shipbuilding assembling stage of joining stiffeners to horizontal flat panels, where the working area is long and narrow. Based on this industrial configuration, it is intended to reproduce the welding position PB (EN ISO 6947) or 2F (AWS A3.0.), during the manufacture of reinforced flat panels, with the final objective of increasing productivity and guarantee the weld quality. Specifically, this paper focuses on the application of HLAW to obtain full penetration T-joints in shipyard environment.

According to the before mentioned studies, HLAW process has been applied to weld T-joints mainly under 1F position. As 2F position is required by real industrial needs, in this contribution, HLAW has been applied to weld fillet joints with 2F position. Concisely, this article shows and analyses the shape characteristics of the single-step T-joints without sealing root made with HLAW process on 8 mm thick EH36 steel plates. Evidences of process improvements are reported in literature when using edge bevelling and some gap between flange and web. However, zero gap with straight edges (square groove) have been used in the present study to simplify the edge preparation and positioning, in order to be able to reproduce easily the welding conditions at industrial conditions.

Similarly, although very low angles of the hybrid welding head are reported in laboratory to provide the best welding conditions to connect flange and web, in the present contribution, reasonable high enough angles of the HLAW head have been employed, to be able to use these welding conditions in real industry.

In addition, a FEM model was developed in order to reproduce the experimental HLAW process applied to the previously described configuration. The three-dimensional simulations provided thermal and mechanical results, allowing the estimations of distortion and residual stresses of the studied structure.

Systematic knowledge of the factors that influence the stability of the HLAW process is of high interest for industrial application. Accordingly, the first objective of the present paper has been to analyse the influence of different HLAW parameters on the weld quality of T-joints. Different processing parameters have been considered, as the laser power, welding speed, filler wire composition, wire feed rate and the configuration of the HLAW processes (laser or arc leading process). To evaluate the welds quality, Non Destructive Tests (NDT) including visual inspection and X-ray tests, metallographic analysis of cross sections, and microhardness mapping tests were performed.

The second objective of the present contribution has been to increase the welding speed, in order to improve the potential global productivity of shipyards. To the author's knowledge, the highest welding rates previously reported for T butt joints with square groove of 8 mm thick steel has been 1.25 m/min [22], 1.1 m/min [3], and 0.6 m/min [27]. Higher welding rates than these values have been tested in the present paper to reach full penetration in one step without sealing root, keeping 2F position and zero gap square groove.

2. Materials and methods

2.1. Materials

Shipbuilding steel EH36 (high strength steels) plates were joined in T-joint configuration in 2F welding position using HLAW processes (Fig. 1). The same 8 mm thick steel plates were used for both web and flange. Plates were cut to pieces of 300 mm × 100 mm (length × width) size, with straight welding edges grid blasted. The surface treatment applied to the welding area of the flange was mechanical milling process. Two types of filler wires were used, both of 1.2 mm diameter, encoded here as FW1 (Filler Wire 1, Union K52 Ni, ER80 S-G according to AWS) and FW2 (Filler Wire 2, WDI 16 SG, ER70 S-6 according to AWS). On one hand, FW1 has a higher nickel amount that allows the weld to reduce the transition temperature from ductile to brittle, thus improving toughness at low temperatures. Furthermore, FW1 contains a low percentage of molybdenum which provides an improvement of the creep resistance of low-alloy steels at high temperatures; this element also produces grain refinement. On the other hand, since the study

Table 1
Chemical compositions of base material (BM, EH36), filler wire 1 (FW1, ER80 S-G), and filler wire 2 (FW2, ER70 S-6) (wt %); Fe balance.

Alloy	C	Si	Mn	Ni	Mo	P	S	Al	Nb	V	Ti	Cu	Cr	Ca
BM, EH36	0.132	0.260	1.400	0.040	0.004	0.009	0.002	0.028	0.036	0.006	0.003	0.012	0.040	0.002
FW1, ER80 S-G	0.060	0.700	1.500	0.900	0.080	0	0	0	0	0	0	0	0	0
FW2, ER70 S-6	0.070	0.875	1.540	0.048	0	0.009	0	0.008	0	0	0	0.120	0.036	0

Table 2
Materials properties (BM, FW1 and FW2) obtained from mechanical tests.

Mechanical test				
Material	Charpy 20 °C (J)	Yield Strength (Mpa)	Ultimate Tensile Strength (Mpa)	Elongation (%)
BM	119	375	500	33
FW1	140–150	460–500	560–590	24
FW2	90–100	420–460	520–560	24–27

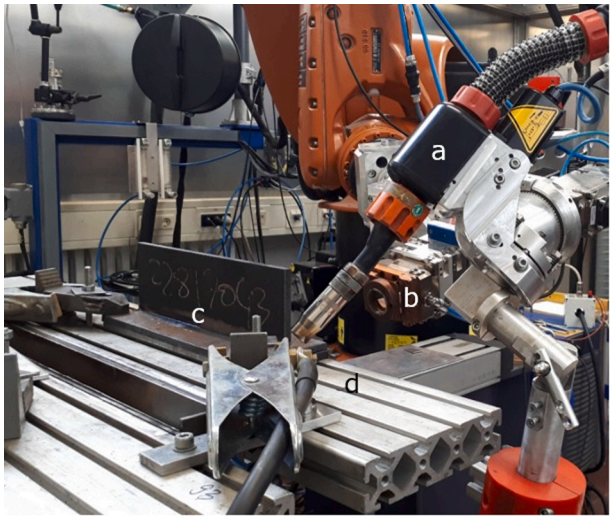

Fig. 2. Experimental configuration: (a) GMA torch, (b) laser beam head (c) sample and (d) electric worktable.

focuses on the application in the naval sector, the FW2 wire was selected because it contains copper, alloying element that favours the behaviour against atmospheric corrosion. In the case of base metal, sulphur and phosphorous levels are kept very low to reduce quenching embrittlement and increase toughness and transverse ductility. Besides, in applications where high toughness is required, small additions of aluminium can be added for grain refinement [34]. Table 1 shows the chemical compositions of base material (BM) and filler wires (FW1 and FW2). Table 2 reports mechanical properties of these materials.

2.2. Experimental procedure

The laser used to carry out the welding tests was a 16 kW TruDisk 16002 disc laser, with a wavelength of 1030 nm and a beam product parameter of 9 mm × mrad. The laser beam was transmitted by an optical fiber with a core diameter of 200 μm. The beam diameter at focal position is 420 μm. A microprocessor-controlled welding machine Qineo Pulse 600 with a maximum current of 600 A was applied as a power source for the arc. The experimental configuration, developed at BAM facilities (Berlin, Germany) is shown in Fig. 2. The welds were made with a flexible laboratory hybrid setup which uses decoupled configuration of the GMA torch (Fig. 2 a) and laser beam source (Fig. 2 b) and allows to adjust their relative position. The whole hybrid head has an approx. size of 73 cm (length) × 12 cm × 12 cm, including the collimating lens and the focusing lens. The samples (Fig. 2 c) were welded keeping the hybrid head fixed, moving the worktable (Fig. 2 d). The position of the welding optics remained constant during the process. A mixture of 82% Argon and 18% CO_2 (commercial name Corgon 18), was used as shielding gas, which was driven by the GMA torch nozzle with a flow rate of 18 l/min.

Before performing the hybrid welding tests, the plates were held by tack welds at both ends and in the middle of the welding path, in order to fix the vertical plate. The tack welds are made with the SMAW method with coated electrode.

The HLAW T-welding process under 2F welding position required a meticulous systematic methodology. Firstly, the laser beam is positioned by adjusting the angle of incidence and the position of the focal point. Secondly, the working angles of the GMA torch are configured as well as the parameters corresponding to the arc process. The heat input of the

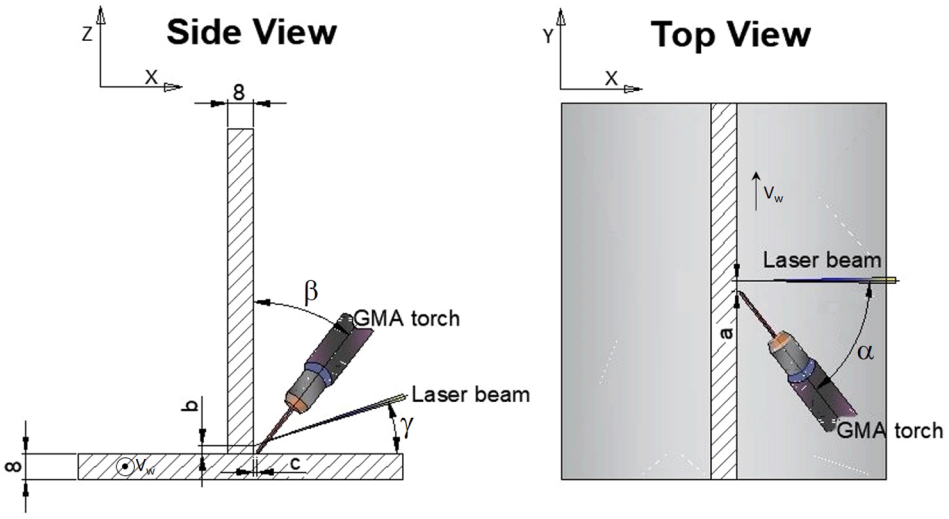

Fig. 3. Geometric configuration of Laser & GMA sources to workpiece.

Table 3
Process parameters of HLAW tests.

Test number	1	2	3	4	5	6	7	8	9	10	11
Filler Wire	FW1							FW2			
α (°)	30	30	23	23	23	23	23	26	26	26	26
β (°)	30	45	38	38	38	38	38	31	31	31	31
γ (°)	20	30	18	18	18	18	18	12	12	12	12
Distance laser-arc, *a* (mm)	4,5	4,5	4,5	4,5	4,5	4,5	4,5	3,5	3,5	3,5	3,5
Offset laser, *b* (mm)	3	4,5	2,5	2,5	3	3	2,5	1	1	1	1
Offset GMA -joint, c (mm)	0	0	0	1	1	1	0	0	0	0	0
Laser Power (kW)	7	7	7	7	7	8	7	7	8	9	10
Source leading	Arc	Arc	Arc	Arc	Arc	Arc	Laser	Laser	Laser	Laser	Laser
Welding speed (m/min)	1,8	1,8	1,8	1,8	1,8	1,8	1,8	1,9	1,9	1,9	2,2
Filler wire feed rate (m/min)	12	12	14	14	14	14	14	14	14	14	15
Intensity (A)	N/A	N/A	N/A	354	353	356	N/A	356	344	353	375
Voltage (V)	N/A	N/A	N/A	32.5	33.2	32.4	N/A	33.5	33.5	33.6	34.7

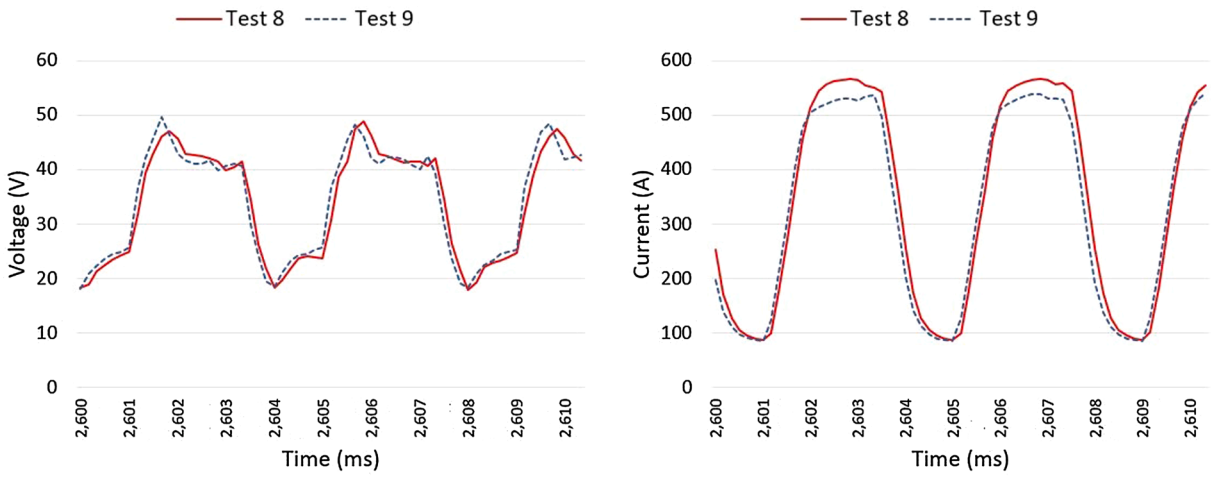

Fig. 4. Voltage and current signals registered during the GMA welding analysis for Tests 8 and 9.

laser beam and the GMA process is adjusted through the laser power, the welding speed, and the power of the electric arc source (adjusting the arc current and the voltage).

The geometric configuration of laser and arc sources were fitted to the workpiece, considering different parameters to control the position and angles (Fig. 3). The angles considered were (Fig. 3): the top view angle between laser beam and GMA torch (α), the angle of incidence between the GMA torch and the web (β), and the laser beam incidence angle from flange (γ). The further geometrical positioning parameters were (Fig. 3): the working distance between the laser beam and GMA torch (*a*), the vertical laser offset distance from the flange (*b*), and the horizontal GMA offset distance from the web (*c*). In all welding experiments, the tip of the GMA filler wire was placed exactly in the joint, the stickout was set to 16 mm and the focal point position was −3 mm.

All joints were welded in T-joint configuration with technical 0 mm of gap. The laser power varied in the range between 7 kW and 10 kW, and the welding speed was in the range of 1.8 m/min to 2.2 m/min. The filler wire feed rate was also tested with the following values: 12 m/min and 15 m/min. The summary of the welded specimens is shown in Table 3. Note that the first set of welding experiments were performed with FW1 (Tests 1–7), while the second group of welds, with FW2 (Tests 8–11).

The arc current was in a pulsed mode, allowing a better control of the geometry of the weld bead and the behaviour of droplet transfer to the molten pool. The final morphology of the weld is closely influenced by the process parameters. The laser source has a great influence on the weld root, presenting a lower effect on weld throat where the filler wire is deposited by the GMA process.

A measuring device for analysing welding processes, WeldAnalyst HKS-P1000, was connected to the arc power source to record the signals resulting from the GMA process. The arc welding parameters were established as follows: pulse frequency, 286 Hz; arc current peak, 563 A; base arc current, 68 A; voltage command value 32 V. Arc voltage and arc current profiles were measured by GMA analysis and revised after welding tests. Examples profiles for Tests 8 and 9 are depicted in Fig. 4, showing the charts registered between 2.600 ms and 2.610 ms.

Preliminary tests were carried out to determine the range of welding parameters, which can be applied for the production of a series of welds with a reproducible quality for further evaluation. Formation of a crater at the end of the seam has been ignored, as this is of secondary importance for industrial scale.

Additionally, a simulation model based on finite element calculations was developed, using SYSWELD software, which estimates the effect of a moving heat source on the joining parts. The FEM model follows thermo-elasto-plastic stages of the welding process, providing thermal results and mechanical effects on the structure. The most interesting thermal outputs were the maximum temperature reached by each node (indicating the nodes belonging to the fusion zone, FZ, to the heat affected zone, HAZ, or to the base metal, BM). Mechanical outputs were also obtained, especially the distortion (displacements of nodes of the mesh) and residual stresses (Von Mises). Meshing of FE nodes in 2D and 3D sections, depicted in Fig. 5 (a) and (b), was defined taking as a reference the geometries of the fusion zone (FZ) of welds. The final mesh consisted of 127,575 3D finite elements, with a greater refinement at the seam, the node distances ranging between 0.13 mm (fusion zone) to 4.38 mm (base metal far from the seam). The global heat source is a combination of a truncated cone Gaussian mathematical model, shown in Fig. 5 (c), to simulate the laser source, and a Goldak's double-ellipsoid

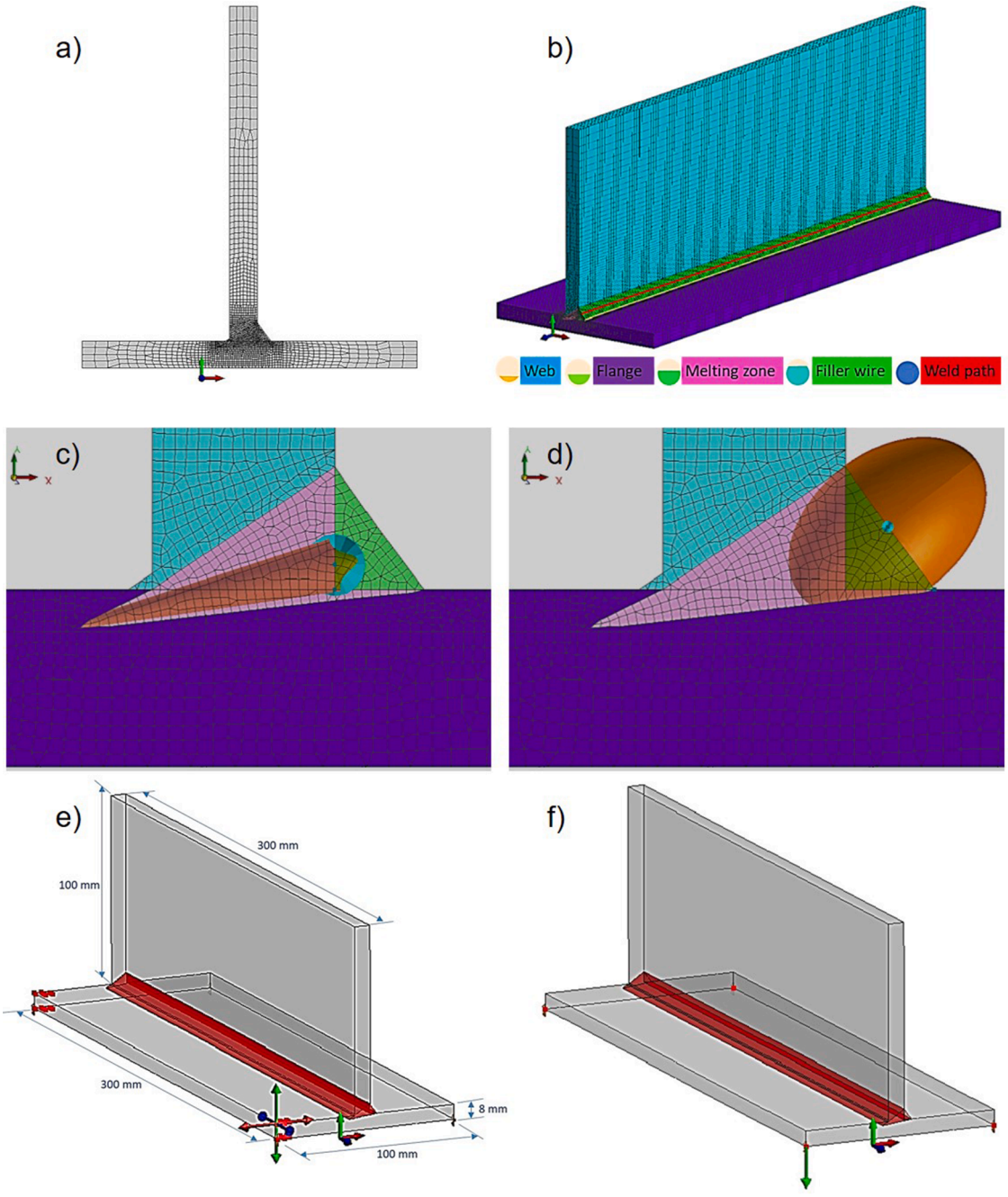

Fig. 5. Details of the FEM model: a) 2D mesh; b) 3D mesh; c) 2D section of Laser heat source; d) 2D section of GMA heat source; e) Welding clamps; and f) Supports after welding.

mathematical model represents the GMA source, depicted in Fig. 5 (d). The size of the combined heat source was carefully fitted taking into account real measurements of the melting pool during the welding process. Both heat sources were combined to simulate the volumetric heat flux distributions of the HLAW process, using the same separation distance between both sources (3.5 mm) as in the experimental welding tests, to get accurate results. The FEM model reproduced the real dimensions of the welding parts (300 mm × 100 mm × 8 mm), joint under 2F position on butt T-joint. Free air cooling condition was selected. Regarding the boundary conditions of the FEM model, clamps and movements restrictions were fixed at the same conditions used in experimental tests. Thus, the nodes located at both left corners of the flange mesh (red points of Fig. 5 (e)) were clamped in all axes (X, Y, and Z axes) during welding and delivered after the process. The movements of the 4 nodes located at the lower surface corners of the flange were restricted at –Y axis after welding (Fig. 5 (f)). S355J2G3 was the material selected from the SYWELD software database to carry out the FEM model, considering this material for both base metal and filler wire, due to their similar thermal and mechanical properties.

Samples welded with different parameters were subjected to deep examinations. The characterisation and evaluation tests were chosen to fulfil the standard quality control tests usually applicable to this T configuration. These tests include visual inspection, radiographic testing (RT) to analyse imperfections of some samples, metallographic evaluation of cross sections and microhardness tests at different locations of welds by microhardness mapping by means of UCI (Ultrasonic Contact Impedance) method as shown in Fig. 6, where each dot represents a single microhardness measurement. The selection of tests applied to

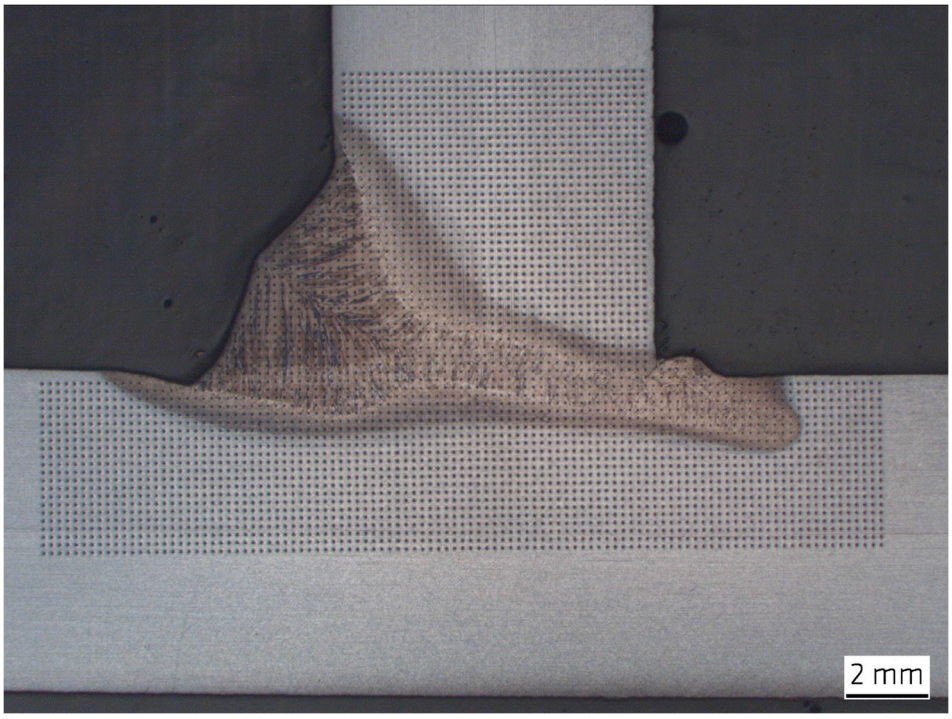

Fig. 6. Example of microhardness mapping of cross section of Test 10 (Each dot is a microhardness measurement).

Fig. 7. Image of weld seam of a HLAW T weld. a) Face side; b) Root side.

each weld was rationally increased as a function of the tests approval. Thus, only the welds fulfilling visual inspection and NDT tests were subsequently analysed by metallographic analysis. The microstructure of relevant welds was examined by optical microscopy. The dendrites size and shape have been analysed at different Laser and GMA fusion zones. The microhardness mappings were therefore made on the best results obtained from the analysed macrographs.

Despite the fact that some imperfections may be found in macrographic images, ISO 12932 standard [35] considers that different types of imperfections can be accepted if defects are below the established levels required for each weld. Three weld quality levels are classified in order to allow application for a wide range of manufacturing. They are designated by B, C and D, where B level corresponds to the highest requirements.

3. Results and discussion

An example of hybrid laser T-joint sample of EH36 structural steel with a thickness of 8 mm can be seen in Fig. 7. The present study analyses the influence of some experimental variables, such as the hybrid welding head configuration, the relative position of arc and laser sources (laser leading or arc leading process), the filler wire composition, laser power (and consequently the energy density), and the welding rate. The experimental approach followed have allowed us to fit these variables in order to obtain a stable welding process and acceptable quality joints for shipbuilding.

As can be seen in Table 1, the difference between wire 1 and 2 relies on the Ni (and Mo at a lower extent) composition. FW1, presenting 0.9 Ni wt. %, is usually employed to improve ductility and toughness of joints, although provides limited wettability. Filler wire 2 (without Ni) is usually employed to provide a good wettability of the melted material during welding process, consideration especially important in T joints with 2F configuration and zero gap analysed in the present paper.

3.1. HLAW tests performed with filler wire 1

The first set of HLAW tests was performed with filler wire 1 (FW1, Tests 1–7 of Table 3), in order to analyse the influence of different key

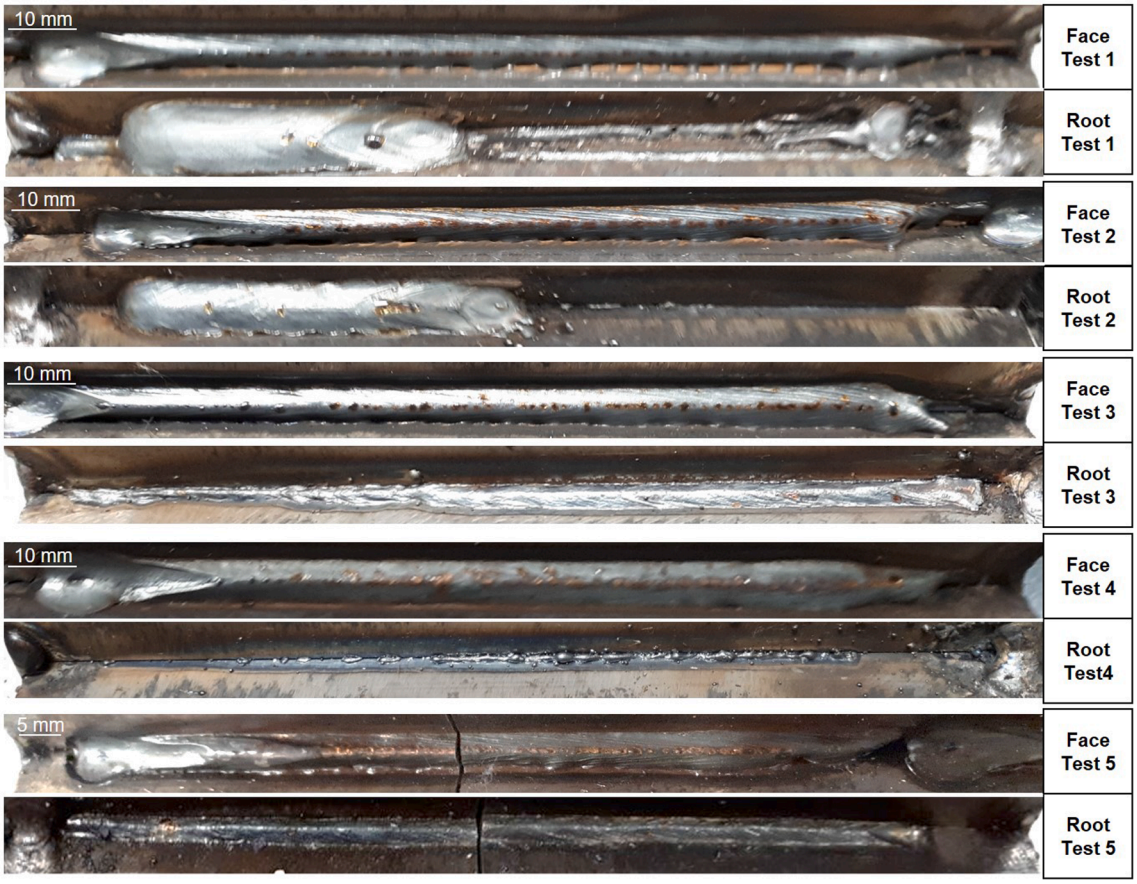

Fig. 8. Macrographic images of face and root sides of HLAW welds obtained in Tests 1–5.

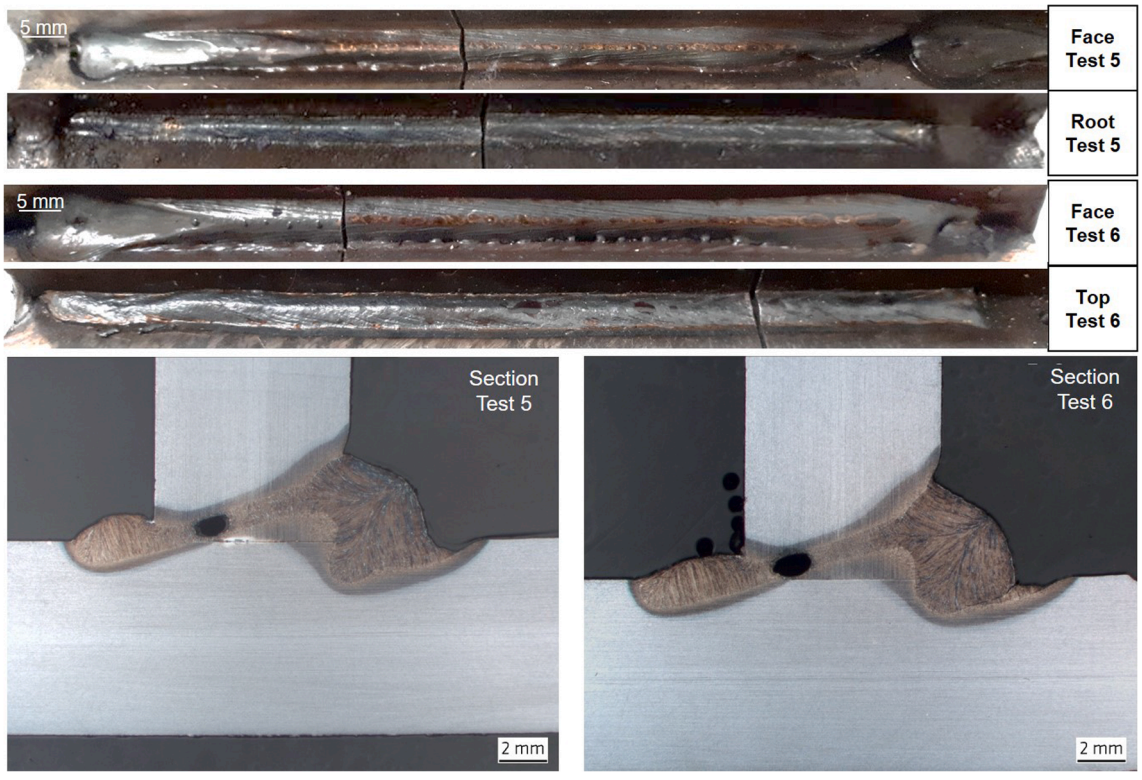

Fig. 9. Macrographic images of face and root sides, and cross sections of HLAW welds obtained in Tests 5 and 6.

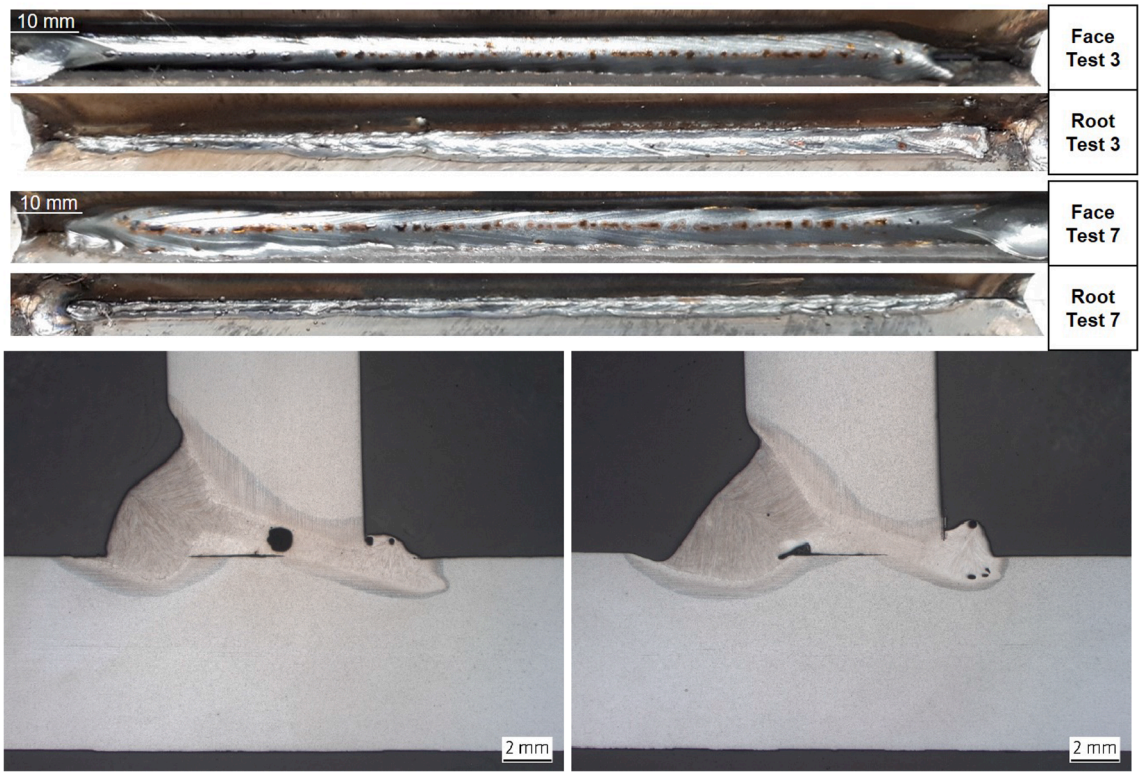

Fig. 10. Macrographic images of face and root sides of T welds obtained in Tests 3 and 7.

experimental parameters, such as welding head configuration (including angles and distance between the arc and laser sources), the laser power, and the relative position of both energy sources (laser or arc leading process).

The influence of the welding head configuration was firstly studied. This includes the analysis of the positioning of both energy sources at the welding zone, controlled by parameters *a*, *b* and *c* (shown in Fig. 3*)*. In these first tests, *b* and *c*, were modified, keeping *a* constant. Additionally, the positioning angles of the welding head (α, β, and γ of Fig. 3) were experimentally changed. Tests 1 to 5 allow one to analyse some of these variables when comparing the results of the obtained welds. Macrographic images taken at the face and root sides of T welds of Tests 1–5, are included in Fig. 8. The welding head configuration of the first weld (Test 1) was fixed according to previous experience of the authors and to some preliminary tests. Test 1 underwent some clear defects identified by visual inspection, as discontinuous undercut, revealing unstable welding conditions. Similar defects are observed in Test 2 (*b*, β, γ were changed), in which lack of fusion at the weld root was also identified. Tests 3 to 5 were performed with reduced values of all angles (α, β, and γ), and different values of *b* and *c*. These changes are seen to improve the welding stability, reflected in the lack of discontinuities previously observed in Tests 1 and 2. However, Tests 3 and 4 still showed some important defects, as high convexity at the weld face, low connection between the flange and web (lack of fusion between both components), and considerable material evolved from the root. Welding conditions of Test 5 improved the connection between flange and web, as high amount of welding material is present between both parts. Note that saw cuts are visible at macrographic images of Test 5.

From these welding experiments, it is clear that low values of angles (specially γ), reduce the defects of HLAW tests performed with filler wire 1. In fact, previous papers published by Udin et al. [23], and Unt, et al. [28] have reported HLAW conditions to join T parts with low γ angles (2.5° and 6°, respectively), obtaining successful results. This consideration based on employing low values of angles sometimes contrasts with the experimental limitations of the HLAW process when intended to be applied at high scale industrial welding. Thus, the welding head, its moving equipment and scaffolds require a minimum working space that can limit the possibility to fit too low values of these angles. For this reason, the value of γ angle employed for all joints of the present paper have been fitted to values equal or above 12 ° , in order to guarantee the real experimental feasibility of using the present results at industrial scale.

The influence of the laser power has also been analysed. Tests 5 and 6 were performed with the same experimental parameters, changing only the laser power from 7 kW (Test 5) to 8 kW (Test 6). Fig. 9 represents macrographic images of face and root sides of these HLAW welds, and cross section images obtained after metallographic preparation of samples. Saw cuts are visible in macrographic images of both welds. Both welds present similar face and root characteristics. The metallographic images of the cross sections revealed some important defects, as the lack of fusion between the flange and the web noticeable for the observable line of separation of both components. A considerable cavity can be clearly observed in these welds, having a size of around 1 mm. The higher laser power applied in Test 6 generates a deeper fused zone at the weld root, but without avoiding the generation of the cavity.

On the other hand, the influence of the relative position of laser and arc sources at the welding head (Arc Leading or Laser Leading process) has been analysed. Tests 3 and 7 were performed with the same welding conditions, excepting the leading source. Thus, Test 3 was carried out with Arc Leading configuration, while Test 7 with Laser Leading configuration. Fig. 10 depicts the external appearance of the 3 and 7 weld tests on both sides (face and root) and the macrosections of both joints. After visual inspection it is observed that the former weld presented a root with continuous excess penetration of melted material. Its welding face shows excessive convexity, excess of material and undercut. Laser Leading weld (Test 7) is characterised by present a narrower root and a welding face with lower curvature. Thus, in visual inspection Laser Leading process presented better results than Arc Leading process, although the overall outcomes were not satisfactory because the macrosections revealed lack of fusion and porosity in both tests.

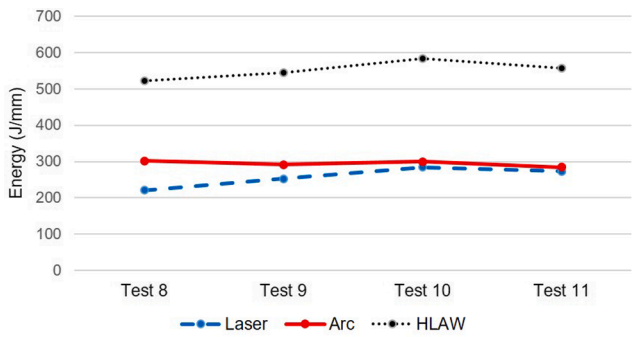

Fig. 11. Comparison of heat input between different welding tests 8 to 11.

From the overall HLAW tests performed with filler wire 1, it can be concluded, that employing low laser beam angle and a 3.5 mm distance between sources has a positive effect on the quality of the T joints with 2F position. In this sense, Liu et al. [7] demonstrated in their experiments that a larger distance between the laser beam and the centre of the arc (4 mm) achieves a spray transfer mode and a more stable welding process than those with reduced distance between heat sources (1 mm), where the transfer mode is globular, and the drop produces a great impact when falling into the melt pool, leading to the formation of porosity in the weld bead. An increase in the laser power leads to deeper penetration welds, the fact which is not necessarily positive if other experimental variables are not properly fitted. Finally, from the comparative analysis of the welds generated at Tests 3 and 7, it can be stated that the Laser Leading process seems advantageous over the Arc Leading for T joints. Similar conclusions are reported in literature [3,5,7]. However, all welds obtained with FW1 suffered from some intrinsic defects, leading to relatively low quality joints, mainly due to lack of fusion, excessive convexity, and the appearance of a considerable cavity at Test 5, 6, 3 and 7 (Figs. 9 and 10).

3.2. HLAW tests performed with filler wire 2

Taking into account the partial conclusions obtained in the previous

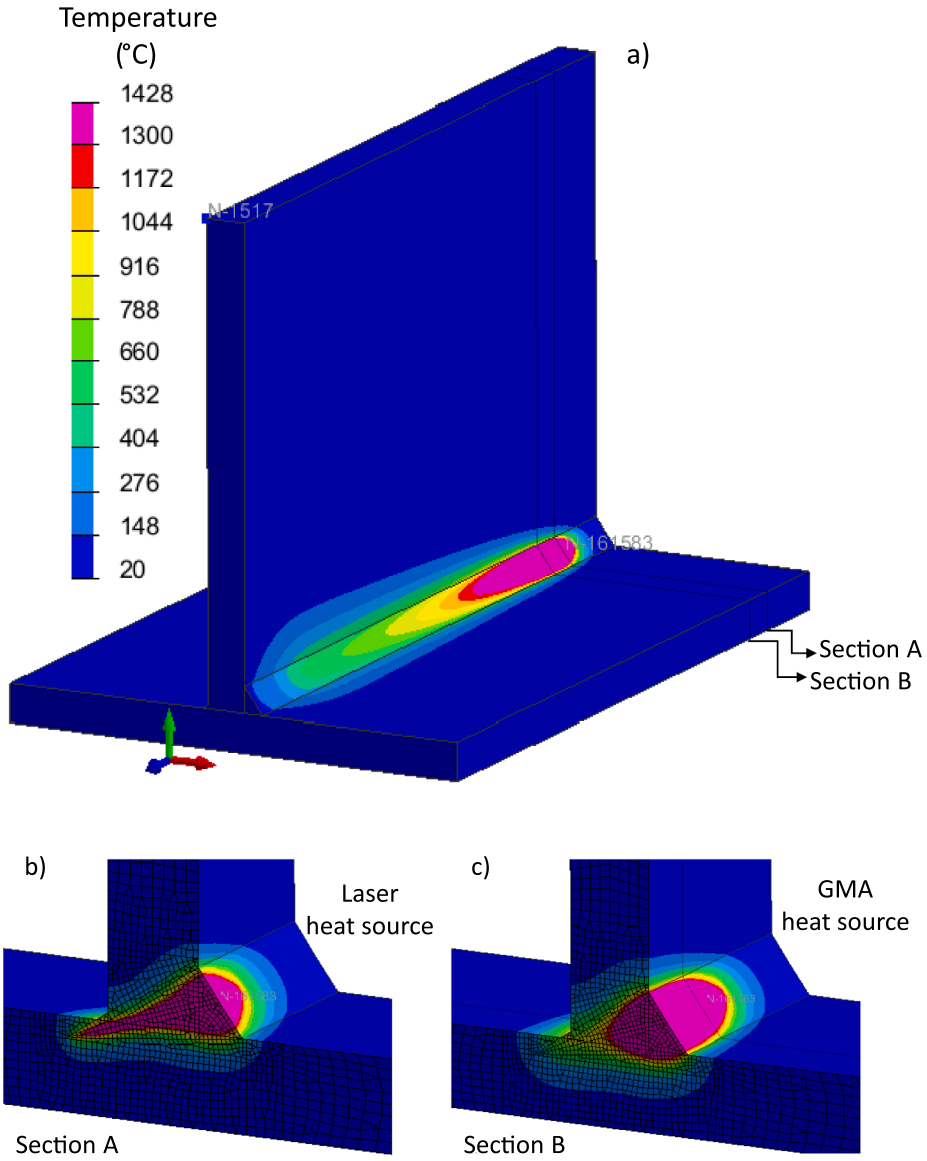

Fig. 12. a) Temperature changes estimated by FEM as the global heat source reaches the end of the joining parts; b) 2D view of the centre of the laser heat source (section A); (c) 2D view of the centre of the GMA heat source (section B).

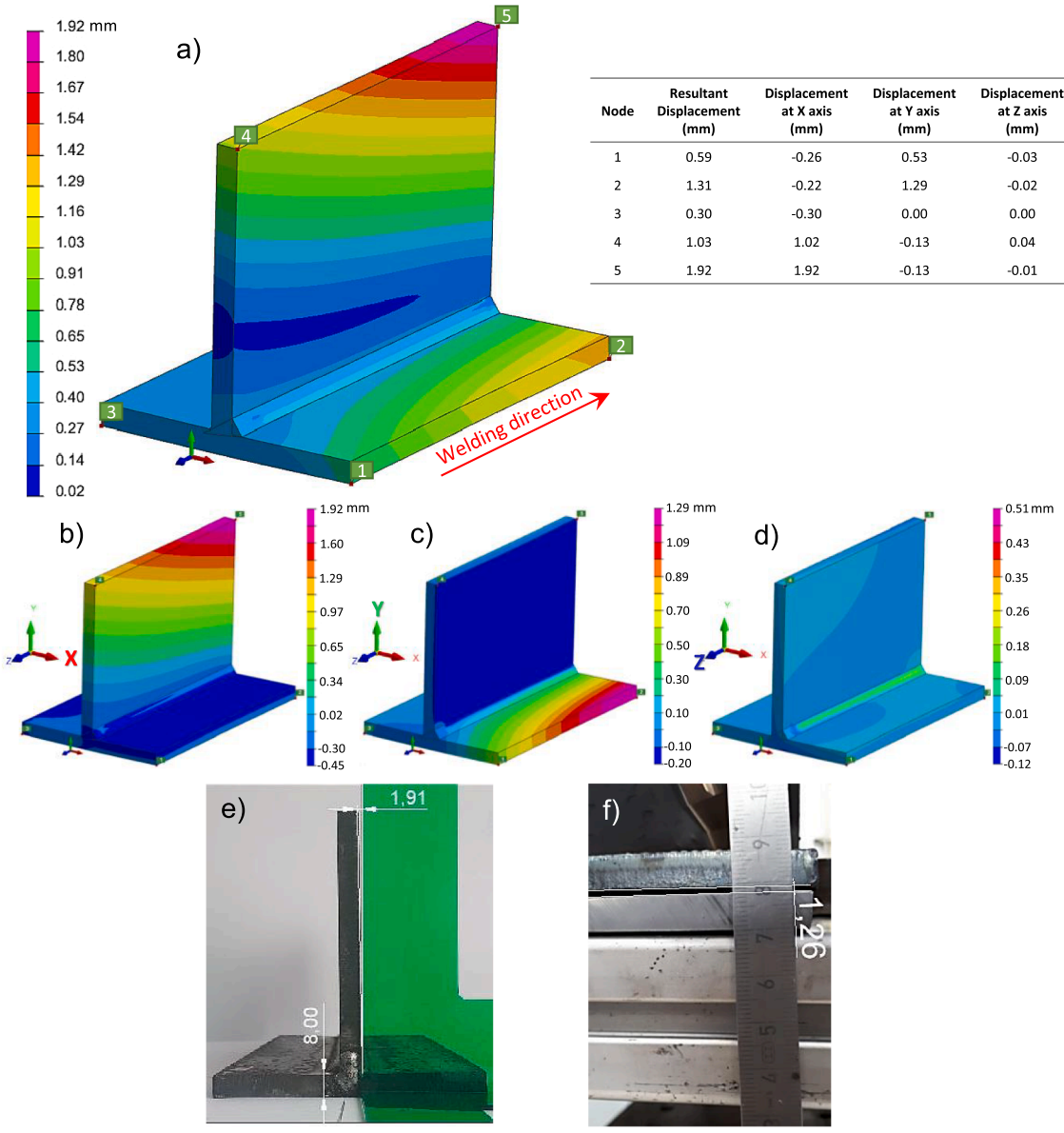

Node	Resultant Displacement (mm)	Displacement at X axis (mm)	Displacement at Y axis (mm)	Displacement at Z axis (mm)
1	0.59	-0.26	0.53	-0.03
2	1.31	-0.22	1.29	-0.02
3	0.30	-0.30	0.00	0.00
4	1.03	1.02	-0.13	0.04
5	1.92	1.92	-0.13	-0.01

Fig. 13. Distortion values of test 10 obtained by FEM (a-d) and by real experimental measurements (e-f). (a) General view of resultant displacement distribution, including displacement values of nodes encoded as 1–5; (b) 3D displacement isometric view with respect to the X axis; (c) 3D displacement isometric view with respect to the Y axis; (d) 3D displacement isometric view with respect to the Z axis; (e) Real measurement of web distortion with respect to X axis at the end of the welded sample; (f) Real measurement of flange distortion with respect to Y axis at the end of the welded sample.

section, and the information reported from published literature, a second set of experiments (Tests 8–11) was developed to improve the quality of welds. Concisely, the following variables were changed: a different filler wire (FW2) was employed, the head angles were decreased to reasonable low values ($\alpha = 26°$, $\beta = 31°$ and $\gamma = 12°$), and Laser Leading configuration was kept for all these new welding tests (Table 3). The influence of the laser power and the welding rate have been analysed.

To analyse the influence of the laser power in HLAW tests performed with FW2, Tests 8, 9 and 10 were considered, providing laser power values of 7, 8 and 9 kW, respectively. Additionally, Test 11 was run in order to weld at a higher processing rate than previously reported in the literature for this HLAW configuration. Thus, the maximum welding speed already achieved in previous works have been 1.25 m/min [22], 1.1 m/min [3], and 0.6 m/min [27]. A similar range of welding speeds (1 m/min and 1.25 m/min) were used by Valdaytseva et al. [36] in their experiments to weld T-joints of 8 mm thickness of AH36 material using autogenous laser welding with a laser beam inclination of 10° and 15° (achievable for the industry). Nonetheless, full penetration was not reached. In the present paper, HLAW weld performed in Test 11 was increased to 2.2 m/min, a 1.76 times faster than those reported previously. This high welding rate requires to increase both the wire feed rate and the laser power to keep the welding process stable. The higher wire feed rate is needed to provide enough feeding material to work at this high rate. Meanwhile, the laser power increase is also necessary to provide enough and controlled energy and to guarantee a full penetration. Thus, the feeding rate was increased to 15 m/min, to work at this high welding speed, the power laser has been fitted to 10 kW to produce a clean seam root (Table 3).

As commented above, the stability of the HLAW process strongly depends on the global energy supplied. Fig. 11 reports the calculation of the heat input values of the 4 welds generated with Tests 8–11, estimated by adding the laser energy to the arc process energy. From Tests 8–10, the heat input grows at a rate of 5% per kW. As explained before,

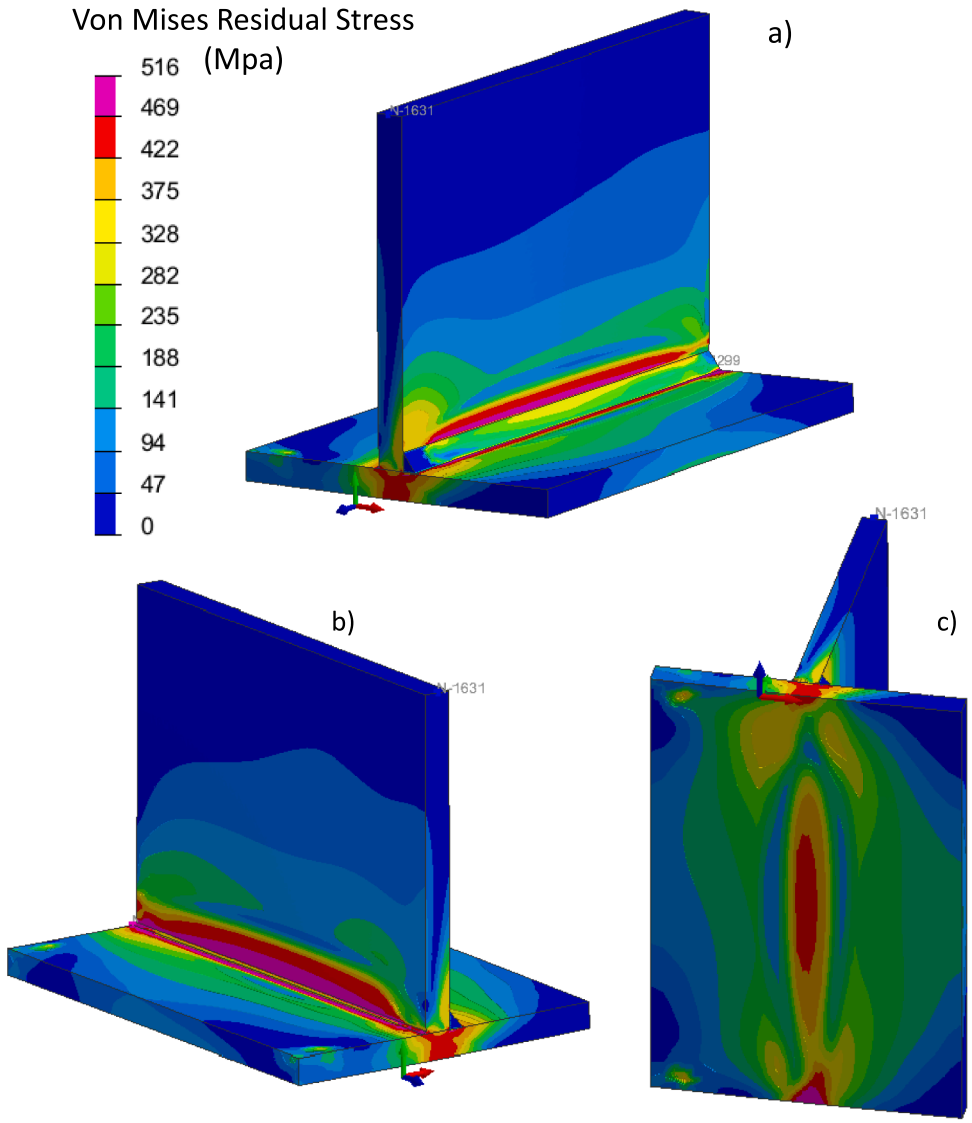

Fig. 14. Von Misses residual stress estimated by the FEM simulations. a) Seam side view; b) Root side view; c) Bottom view of flange.

Test 11 is performed at higher welding speed, leading to a reduction of heat input when compared with Test 10.

FEM simulations were developed to estimate temperature changes, residual stresses and distortion of welded pieces. Simulation results reported were focussed on Test 10, the hybrid weld performed with the highest heat input (maximum global energy of 584 J/mm, as shown in Fig. 11), and therefore, the condition leading to the highest distortion results. The Fig. 12 (a) depicts the temperature distribution underwent by the nodes as the global heat source is reaching the end of the joining parts. Fig. 12 (b) and (c) show the 2D views of sections A and B, corresponding to the centres of the Laser and GMA heat sources, respectively. Fig. 13 shows the distortion values obtained by FEM (images a-d) and by experimental measurements (images e-f). It can be seen that the displacements in the model are asymmetric due to constraints position on one side of flange. It is worth mentioning that in order to obtain a better accuracy of the deformation prediction, the external clamps were carefully adjusted in the FEM model according to the real experiments. Image (a) depicts a general view of the resultant displacement distribution, including the normal displacement values of the most relevant nodes encoded as points 1–5. Additionally, the box includes the selected nodes on the simulation model that correspond to the marked points (nodes 1 to 5), where the normal displacement (global 3D resultant values), as well as the displacement of these nodes regarding the coordinate axes X, Y and Z, are numerically specified. Images (b), (c), and (d) of Fig. 13 presents the 3D displacement isometric view estimated by FEM, referenced to the X, Y and Z coordinate axes, respectively. Image (e) of this figure shows the real experimental measurements of web distortion with respect to X axis at the end section of welded sample. Meanwhile, image (f) of the figure depicts the flange distortion with respect to Y axis, also measured at the end section of welded sample. The maximum flange distortion is observed at node 2, in which a real displacement with respect to Y axis of 1.26 mm (1.29 mm estimated by FEM) was measured. The greatest distortions were found at the upper edge of the web (node 5), leading to a real maximum deflection with respect to the X axis of 1.91 mm (1.92 mm estimated by FEM). As can the observed, excellent agreement between simulation and experimental values were obtained. Fig. 14 shows the Von Mises residual stresses estimated by FEM, of the welded piece obtained in Test 10. Images (a), (b) and (c) of this Fig. 14 depict the seam side, the root side, and the flange bottom views, respectively. The highest residual stresses values were generated in the central area of the seam, exceeding the elastic limit of the base metal (375 MPa). These residual stresses results are related to the deformation produced in the free edges of the flange and the web.

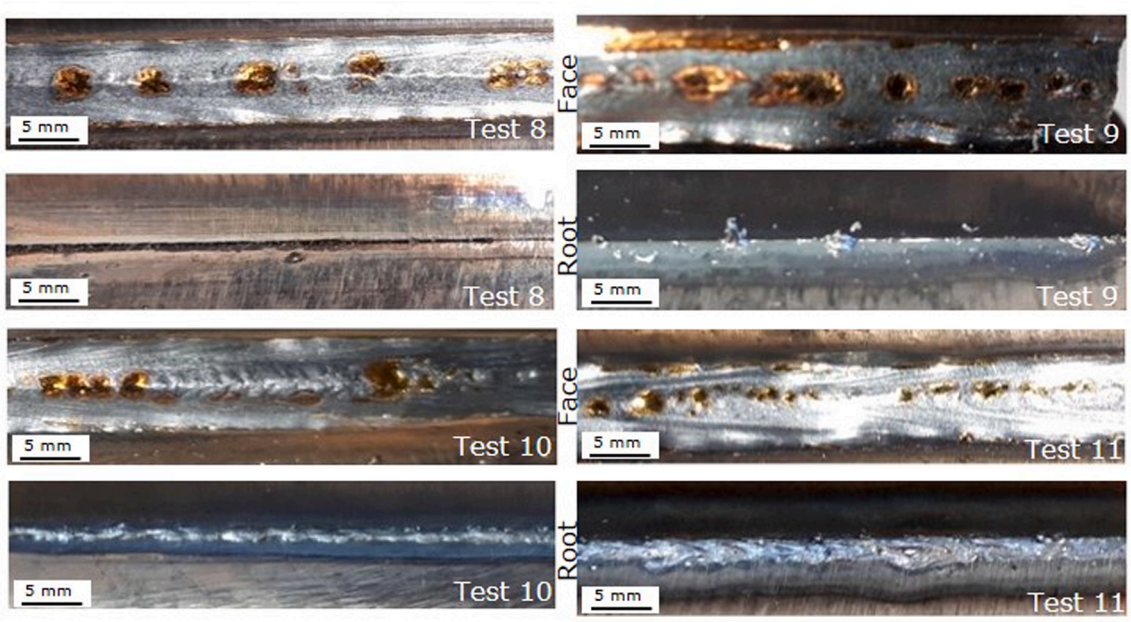

Fig. 15. Details of the appearance of front face and root face of weld beads in T-joints.

Fig. 16. X-Ray test at face side and root side in welded T-joint specimen of Test 10.

The characterisation and evaluation of these welds were carried out by visual inspection, X-Ray analysis, macrographic evaluation of welds cross section, and microhardness measurements.

Fig. 15 shows images of the welds in which the appearance of the seams at representative zones of the specimen can be observed. The front and root side of the seams of each welded sample can be checked. Note that golden stains appearing at face side welds were confirmed by cross sections (not included here) to be superficial. Therefore, they do not appear at inner part of the welds, so they do not risk the mechanical integrity of these welds.

The face side of the weld seam in Test 8 has a suitable appearance, there are no visible defects such as: notches or undercuts. However, the root side reveals lack of fusion and shows incomplete penetration in the joint. Laser power is a key factor in HLAW when the laser is in the forward position, as laser leading generates greater penetration than arc leading position. There is an evidence that increasing the laser power may reach the complete connection. For this reason, Tests 9 and 10 were performed at higher laser power.

Although the visual inspection of the front side of Test 9 should be considered positive, a lack of penetration in the root of the seam can also be detected visually without the need to perform the macro section. Some areas where the seam touches the root begin to appear in this weld.

At Test 10, transitions between the seam and both plates (web and

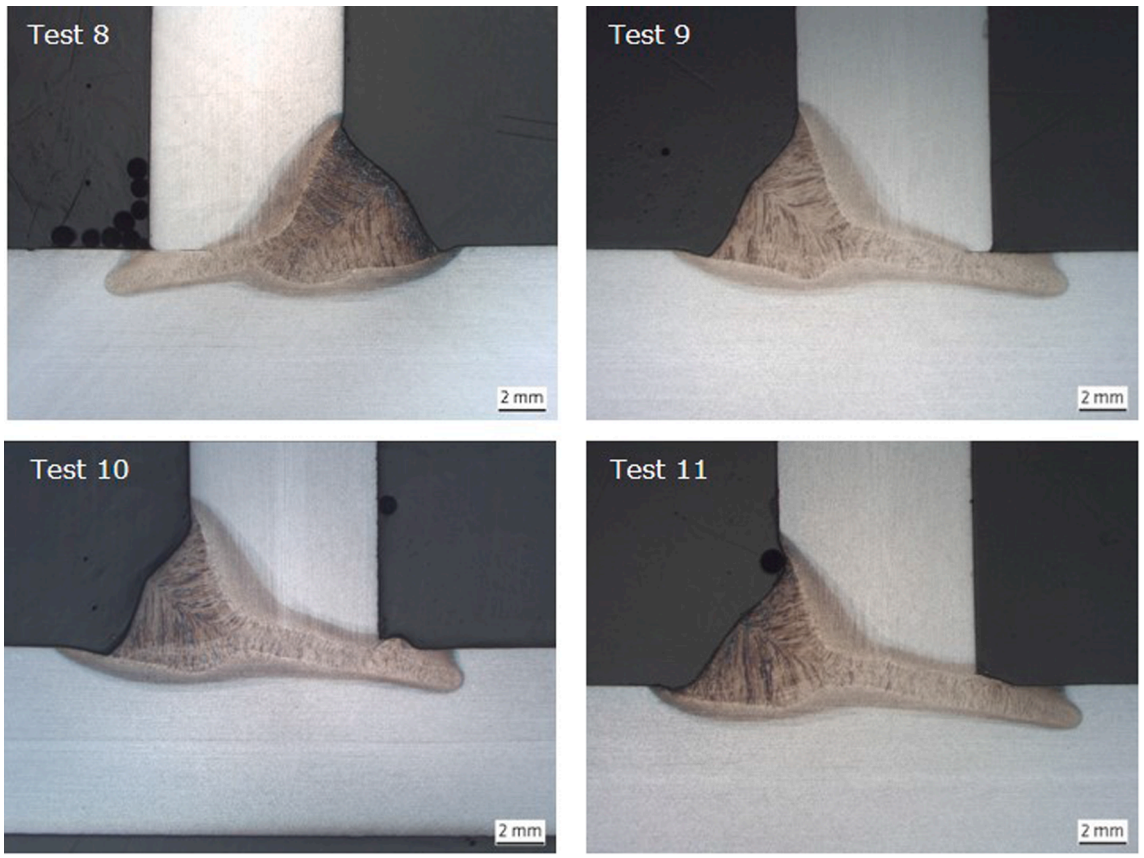

Fig. 17. Macrographic images of cross-sections of HLAW welds obtained from Tests 8–11.

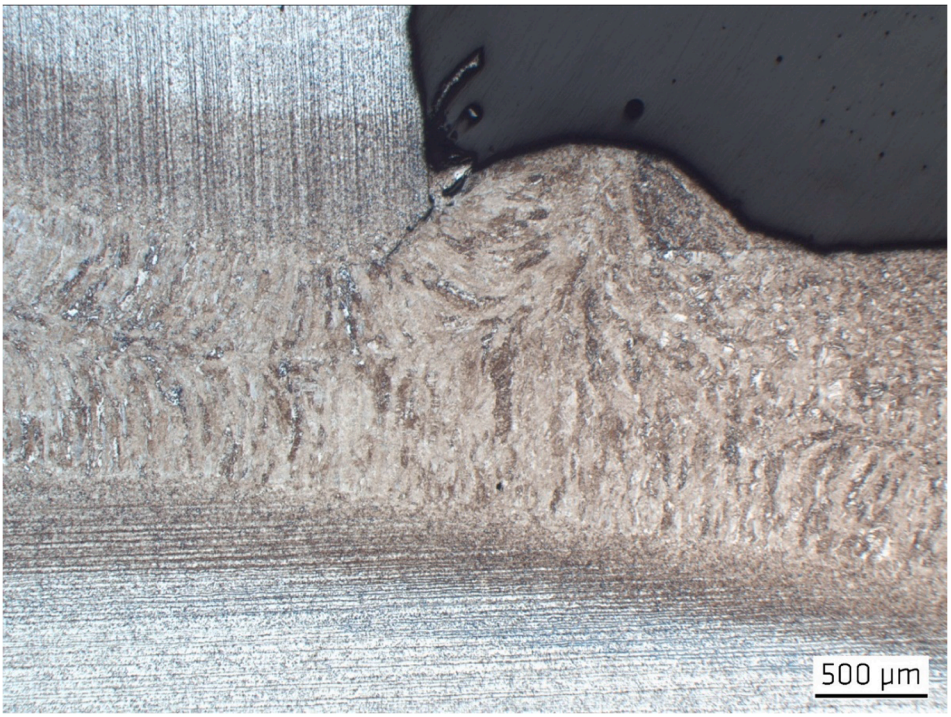

Fig. 18. Lack of fusion in the root zone of Test 10 section.

flange) can be seen without any remarkable notches. In fact, the seam root of this weld shows no signs of lack of fusion. This characteristic of Test 10, in comparison with previous Tests 8 and 9, predicts an improvement in the weld quality. In welding Test 11, the transition between the seam and web (web toe) is smooth, without large undercuts and with a low spatter formation. The root of the seam is continuous.

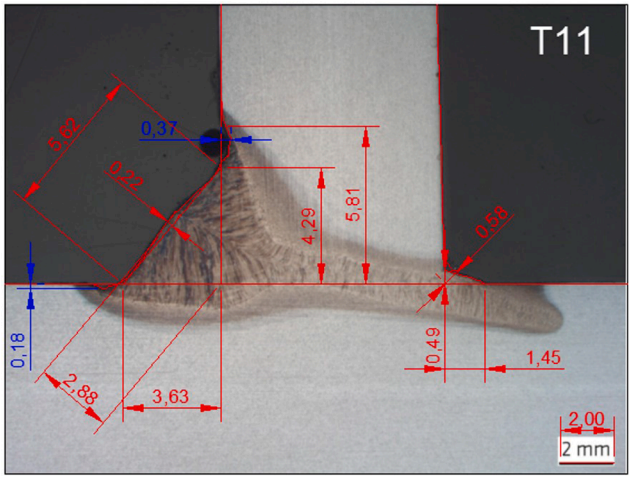

Fig. 19. Detailed imperfections measurements of Test 11.

Fig. 16 shows the results of the radiographic test carried out on the overall length of the welded sample seam of Test 10. The X-ray represents a symmetrical image of the real specimen. No visible welding defects such as cracks or pores are visible in the radiography. A softly darker line above the seam is presented in the X-ray face side image which defines the presence of a light undercut in the web zone. Due to the spot welding carried out to fix the web to the flange, the melt receives an additional material flow which doesn't affect the root of the seam in that area without producing irregularities at this point of the seam. It should be also mentioned that lack of fusion defects could be shadowed due to the path through the material thickness at the zone connecting the web plate to the flange plate.

The macrographic images of the cross sections corresponding to welding Tests 8–11, extracted from the middle part of the bead length, are shown in the Fig. 17. Undercut is usually difficult to avoid in the hybrid welding of T joints. This defect is subsequently measured in these samples.

Comparing the images of welds generated with Tests 8–10, it can be clearly seen that a laser power increase leads to deeper penetration, leading to a better connection between flange and web. Other defects, as cracks or porosities, are not observed. Fig. 18 shows greater magnification of the section made to the Test 10. A reduced zone presenting lack of fusion in the root can be observed.

Test 11 leads to better welding geometry and full connection between flange to web. In fact, the higher welding rate of this test provokes a better integration between both laser and arc sources, which generates a clearer Y weld shape and minimises the gravity effects at the upper fusion zone dominated by the arc process. Another advantage of this weld is the slightly lower size of the arc fusion zone, as lower amount of material and energy are required.

According to the previous results, the welding conditions of Test 11 generates the better quality of T joints, in terms of defect reduction, sound weld geometry and better flange to web connection. An exhaustive analysis of the macrograph of Test 11 was carried out to evaluate the quality level of defects (Fig. 19), not finding internal imperfections or those related to the geometry of this T-joint, such as misalignment or imperfect root. From a superficial point of view, no cracks, pores or lack of fusion were appreciated. A slight continuous undercut was observed throughout the bead. The undercut was measured at different points of the bead using welding gauges and metallographic measurements (values indicated in blue at Fig. 19). All values obtained from the undercut measurement were below the maximum limit required for B quality. Thus, the maximum values allowed by [35] is 0.5 mm or $h \leq 0.05$ t (being h the maximum undercut allowed and t the plate thickness). In this case, 0.4 mm is the reference value for butt T-joints of 8 mm thick. The maximum undercut value measured was 0.37 mm. Therefore, the undercut presented by the samples is allowed by the standard, confirming that the present welding procedure is adequate.

Cross sections of Tests 10 and 11 were subjected to deep metallographic analysis by optical microscopy to study the microstructure developed at different zones of the samples, encoded as Laser and GMA zones, as showed in Fig. 20 (a). Fig. 20 (b-e) depicts micrographic images at 50x of Laser and GMA fusion zones of both Tests 10 and 11. A dendritic growth from the base metal towards the centre of the weld is observed in both Laser and GMA zones. The size and shape of these dendrites are dependent on the solidification conditions of each zone. The laser zone is dominated by smaller and narrower dendrites, as a consequence of the faster solidification. In contrast, GMA zone presented larger and wider dendrites, encouraged by the slower cooling of the weld pool. The mean width of these dendritic formations have been measured and reported in Fig. 20 (f). In all samples, the mean width values measured at Laser fusion zones are clearly lower than those measured at GMA zones. It is interesting to note that Test 11 provided lower values for both zones than Test 10. This fact is related to the lower heat input of Test 11 (Fig. 11), encouraging a faster cooling rate of the fusion zone, generating smaller dendrites.

Fig. 21 (a-d) depicts micrographic images at higher magnification (500x) of Laser and GMA fusion zones of these Tests 10 and 11. The microstructure of the fusion zone presented elongated needle shape ferrite grains (light colour). A clear microstructure refinement is observed at Laser zone if compared with the GMA in both welds, as a consequence of the higher cooling rate of the former zone. The refinement of the grain makes the steel microconstituent stronger, tougher and more uniform as a whole [34].

Both welds of Tests 10 and 11 were subsequently subjected to microhardness mapping. Fig. 22 shows the microhardness map obtained from HV0.5 Vickers tests at weld samples of Test 10 and Test 11, the samples providing the overall best results in previous tests. Microhardness mapping of both samples presented very similar values distributions. Two different fusion zones are clearly identified at both samples, the upper part, dominated by the arc process, and the lower part, mainly affected by the laser source. The arc zone present lower hardness values than 300 HV. It is also worth mentioning that the zone connecting the flange and the web presents lower microhardness values than 380 HV, values generally accepted by the standard applicable naval and material regulations, such as ISO 15614-14 [37], Bureau Veritas NR 216 DT R10 E [31] and, Lloyd's Register Rules for the Manufacture, Testing and Certification of Materials [32]. These regulations limit the highest allowed hardness values of welded zones at 380 HV (as stated by ISO [37]) and 420 HV (according to BV and LR [31,32]). The laser zone appearing at the weld root presented higher hardness values than 380 HV due to the higher cooling rate, leading to stronger microstructure. However, this characteristic is not considered here as critical, as this high hardness zone are out of the flange-web connection. It seems that higher welding speed provokes high hardness values at the root of the HLAW weld. In the same way that Bunaziv et al. [19] showed in their study, a substantial increase in hardness can result from the rapid cooling rate in the root area when a laser energy source in a welding process is applied. The microstructure and, therefore, the microhardness can be smoothed by decreasing the welding speed, by increasing the welding heat input, and/or changing the chemical composition of the filler wire, as recommended by Ramkumar et al. [5]. Future research can be focussed on these process changes, in order to smooth the microstructure of the weld laser zone, which can reduce the maximum hardness values measured at this zone.

The overall HLAW experiments performed and analysed in the present paper have allowed us to analyse the influence of different welding parameters, and to define a procedure able to achieve high quality T joints with 2F configuration. The second sets of welding experiments, performed with FW2, lower head angles, and laser leading configuration, have provided clearly better results. The filler wire used seems to

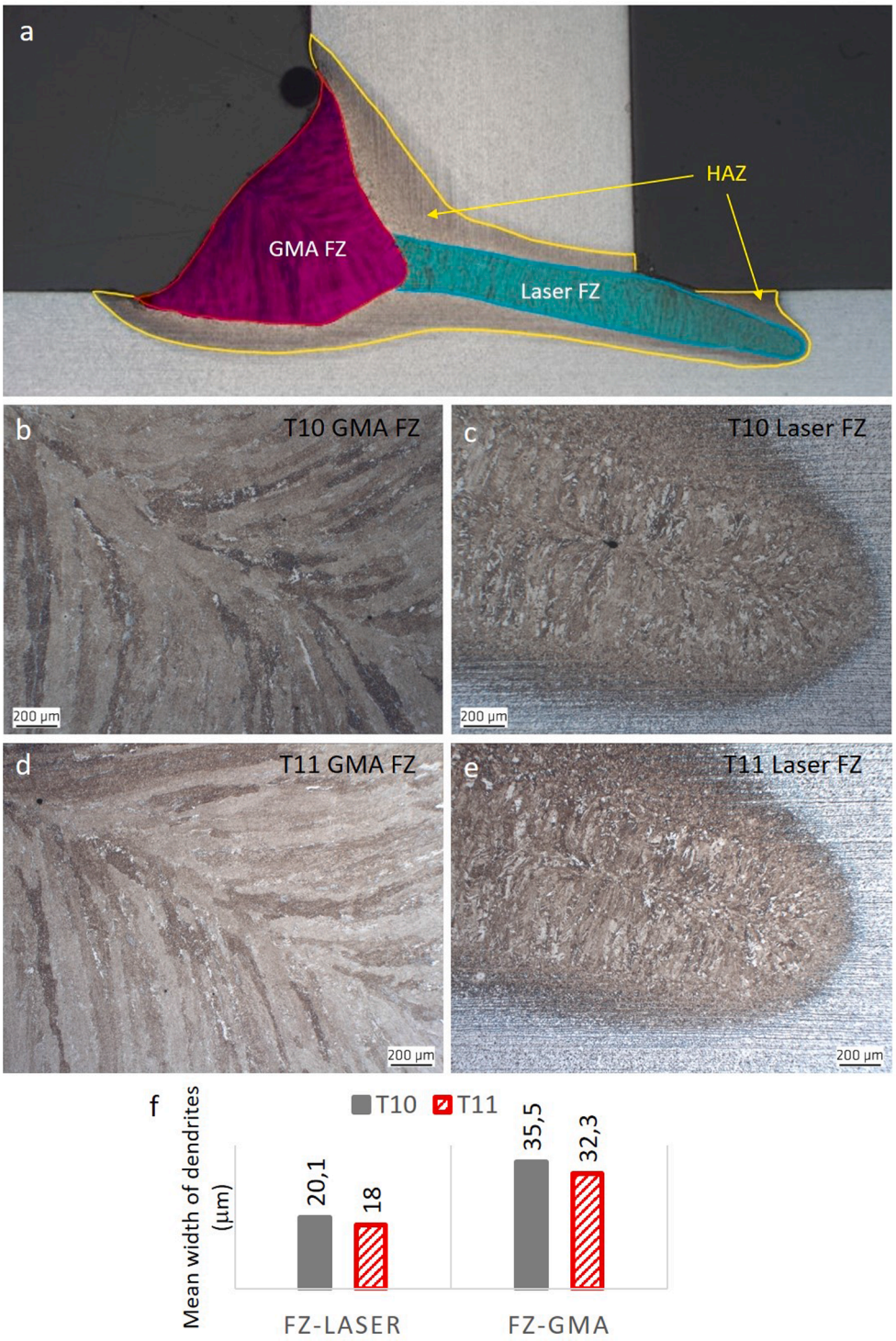

Fig. 20. Microstructural analysis of welds obtained at Test 10 and Test 11. (a) Identification of GMA and Laser fusion zones of T HLAW weld (Test 11). (b-e) Micrographic images at 50x of Laser and GMA fusion zones. (f) Mean width values of dendritic formations at Laser and GMA fusion zones.

be a key issue in HLAW experiments. In comparison with FW1, FW2 welds normally presented a smoother transition between flange and web, leading to lower convexity seams. This fact is thought to be associated to the improved wettability properties of FW2, although further research is needed to confirm this. Other influencing factors observed experimentally are the welding head configuration (including angles and distance between the arc and laser sources), laser power and source leading (laser or arc leading process).

In comparison with the studies previously published in the scientific literature for this configuration, the present paper has successfully implemented the following process advantages: only one step process without sealing root for this type of material (EH36-N steel), use of straight edges without gap between flange and web, and higher welding rate than previously reported.

Regarding the edges preparation issue, it is true that previous works have already obtained high quality HLAW T joints when using a groove at the web and or leaving a gap between both components. This gap encourages the access of filling material at the welding zone.

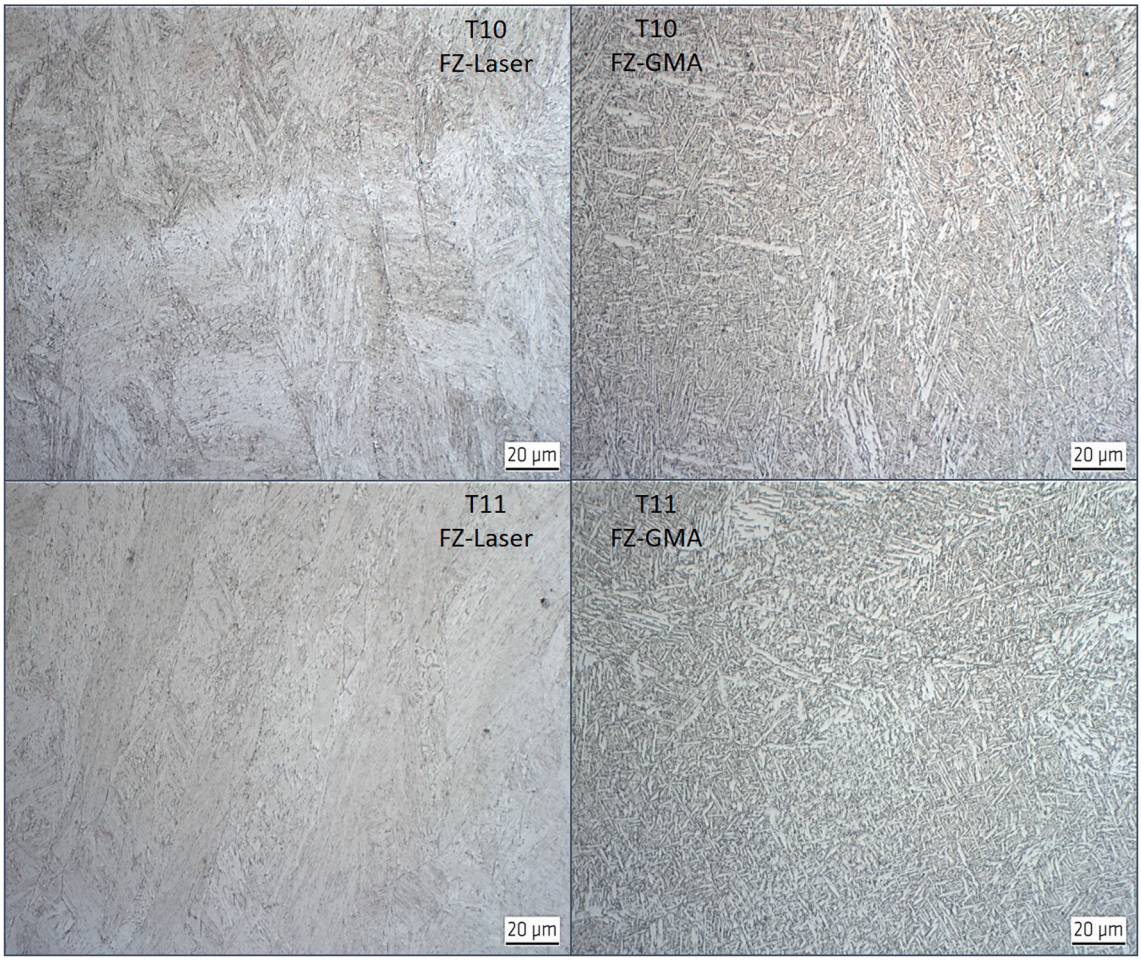

Fig. 21. Micrographic images at 500x of fusion zones of HLAW welds obtained in Tests 10 and 11.

Nevertheless, few investigations have already tried to weld this T structure without gap and leaving the straight edges (with flat milling preparation). This edge preparation is in fact an actual industrial requirement for being easily implemented, although it is obviously a challenge for the HLAW process, as the access of filler wire material is limited. As far as the authors are concerned, the present paper is the first research paper reporting a welding procedure in which straight (flat milled) edges are used in HLAW T joints of 8 mm thick.

On the other hand, in the welding procedure employed in Test 11, the welding rate was able to be fitted at 2.2 m/min, getting a faster HLAW process than those previously published in the research literature for this T welds with 2F configuration. In fact, previous papers reported welding rates up to 1.25 m/min for T butt joints with square groove [22]. Therefore, an increase of 1.76 times in the welding rate was able to be successfully employed in the present paper, obtaining welds fulfilling the applicable quality control tests for this welding configuration (including visual inspection, inspection by non destructive tests, macrographic evaluation of cross sections and microhardness tests).

4. Conclusions

In the present paper, HLAW process have been employed to weld EH36 steel of 8 mm thickness, for T butt joint configuration with square groove, on 2F welding position. This research is highly demanded by the industry, as very few studies reports investigation of this real configuration.

Two main objectives have been covered: 1) analyse and fit the different processing parameters, as the laser power, welding speed, filler wire composition, wire feed rate and the configuration of the HLAW processes (laser or arc leading process) and 2) increase the welding speed.

The second sets of HLAW welds, performed with Filler Wire 2, with laser leading configuration, high laser power, and with low head angles (γ and b), have provided the best joints quality. These welds fulfilled the standard quality control tests required by naval industry [31,35,37], including Non Destructive Tests, metallographic analysis of cross sections, and microhardness mapping tests.

FEM simulations performed with SYSWELD have allowed the estimation of temperature distribution changes at different welding zones, the web and flange distortion values, and Von Mises residual stresses. An excellent agreement between simulation results and experimental distortion measurements was obtained.

As far as the authors are concerned, full penetration 8 mm T welds were successfully obtained for the first time at industrially applicable 2F position with reasonable HLAW head angle (12° from flange), in one single step without sealing root, and using 0 gap square groove edge preparation. The present contribution presents welding rates up to 2.2 m/min for 2F T joints of this steel thickness, a 1.76 times higher than previously reported at the revised literature.

CRediT authorship contribution statement

C. Churiaque: Methodology, Software, Validation, Investigation, Writing - original draft, Writing - review & editing, Visualization. **J.M. Sánchez-Amaya:** Conceptualization, Data curation, Writing - original draft, Writing - review & editing, Supervision, Project administration. **Ö.**

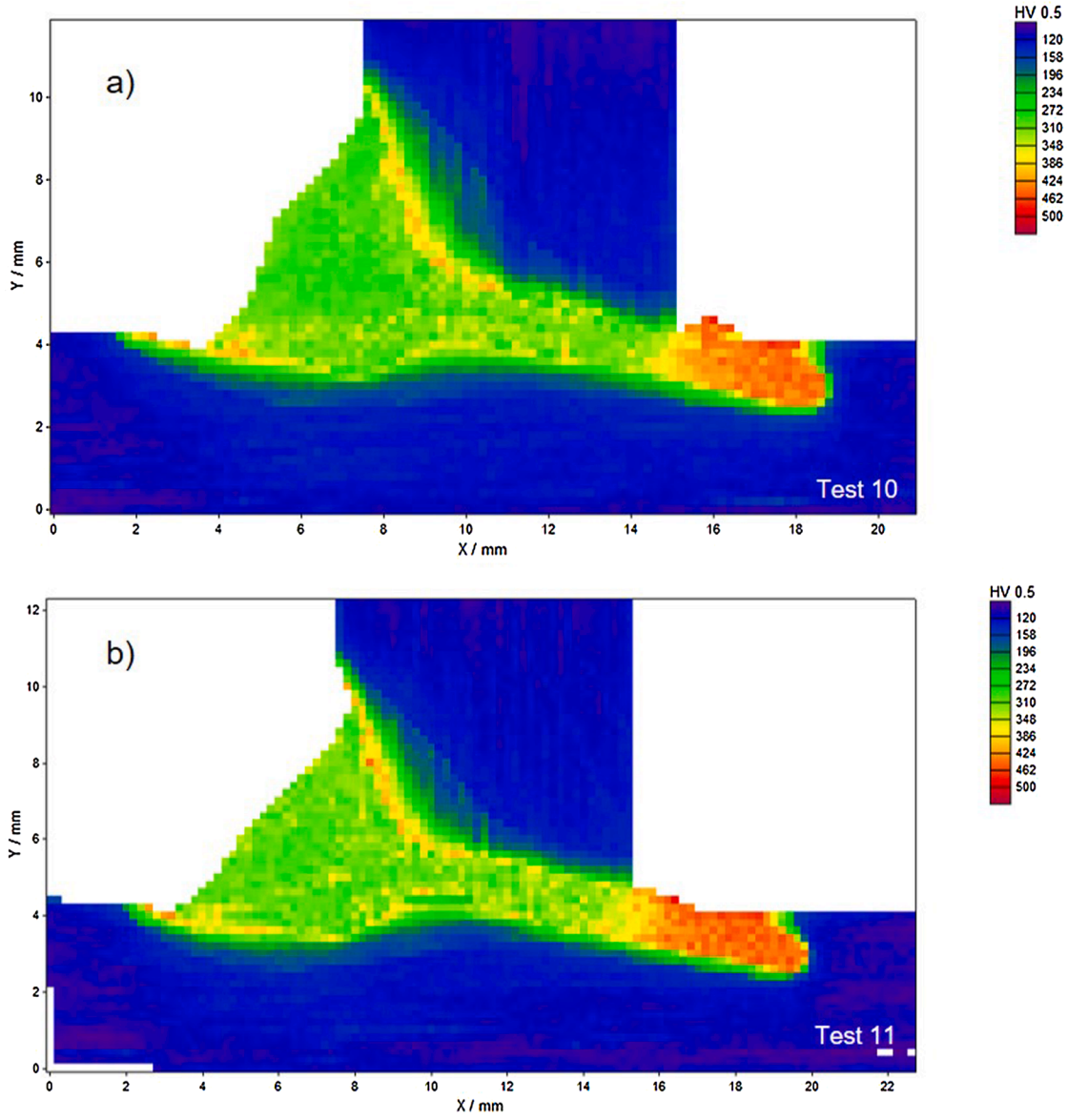

Fig. 22. HV 0.5 Vickers microhardness map performed at welds of Test 10 (a) and 11 (b).

Üstündağ: Methodology, Investigation, Visualization. **M. Porrua-Lara:** Resources, Funding acquisition. **A. Gumenyuk:** Conceptualization, Investigation, Resources, Writing - review & editing, Supervision, Funding acquisition. **M. Rethmeier:** Conceptualization, Resources, Writing - review & editing, Supervision, Funding acquisition.

Declaration of Competing Interest

The authors declare that they have no known competing financial interests or personal relationships that could have appeared to influence the work reported in this paper.

Acknowledgements

The present paper belongs to C. Churiaque's PhD. She would like to thank to the Vicerrectorado de Política Científica y Económica of the University of Cádiz and Navantia S.A. S.M.E. for the financial support of her industrial doctoral thesis. She also thanks to BAM for providing facilities and technical support (specially to the technician Marco Lammers) to conduct the experiments included in this communication. In addition, the fellowship covering her stay in Division 9.3 of BAM is acknowledged to the Campus of Global International Excellence of the Sea CEI • MAR.

References

[1] B. Acherjee, Hybrid laser arc welding: State-of-art review, Opt. Laser Technol. 99 (2018) 60–71.
[2] C. Churiaque, M. Chludzinski, M. Porrua-Lara, A. Dominguez-Abecia, F. Abad-Fraga, J. Sánchez-Amaya, Laser Hybrid Butt Welding of Large Thickness Naval Steel, Metals (Basel) 9 (1) (2019) 100.
[3] J. Gorka, Structure and properties of hybrid laser arc welded T-Joints (Laser beam-MAG) in thermo-mechanical control processed steel S700MC OF 10 mm thickness, Arch. Metall. Mater. 63 (3) (2018) 1125–1131.
[4] Ö. Üstündağ, S. Gook, A. Gumenyuk, M. Rethmeier, Hybrid laser arc welding of thick high-strength pipeline steels of grade X120 with adapted heat input, J. Mater. Process. Technol. 275 (2020) 116358, https://doi.org/10.1016/j.jmatprotec.2019.116358.
[5] K.D. Ramkumar, K. Dharmik, B. Noronha, K. Giri Mugundan, S. Bhargav, K. V. Phani Prabhakar, Structure-property evaluation of single pass Laser-arc hybrid welding of resulphurized martensitic stainless steel, J. Mater. Process. Technol. 271 (2019) 413–419.
[6] TWI, 2020. https://www.twi-global.com/what-we-do/research-and-technology/technologies/welding-joining-and-cutting/lasers/hybrid-laser-arc-welding.
[7] W. Liu, J. Ma, G. Yang, R. Kovacevic, Hybrid laser-arc welding of advanced high-strength steel, J. Mater. Process. Technol. 214 (12) (2014) 2823–2833.

[8] J. Ning, L.-J. Zhang, J.-N. Yang, X.-Q. Yin, X.-W. Wang, J. Wu, Characteristics of multi-pass narrow-gap laser welding of D406A ultra-high strength steel, J. Mater. Process. Technol. 270 (2019) 168–181.
[9] S. Olschok, Laserstrahl-Lichtbogen Hybridschweißen von Stahl im Dickblechbereich, Shaker Verlag, 2008, pp. 102–107.
[10] Sanchez-Sotano, A.J. Ramirez-Peña, M., Churiaque, C., Abad-Fraga, F., Sánchez-Amaya, J.M., Salguero, J., 2019. Performance analysis of a flat panel manufacturing line adding hybrid laser welding technology. VII Congreso Nacional de i+d en Defensa y Seguridad. Contribución DESEID-163.
[11] G. Turichin, M. Kuznetsov, I. Tsibulskiy, A. Firsova, Hybrid Laser-Arc Welding of the High-Strength Shipbuilding Steels: Equipment and Technology, Phys. Procedia. 89 (2017) 156–163.
[12] W.-S. Yoo, J.-D. Kim, S.-J. Na, A study on a mobile platform-manipulator welding system for horizontal fillet joints, Pergamon. Mech 11 (7) (2001) 853–868.
[13] Ö. Üstündağ, S. Gook, A. Gumenyuk, M. Rethmeier, Mechanical properties of single-pass hybrid laser arc welded 25 mm thick-walled structures made of fine-grained structural steel, Procedia Manuf. 36 (2019) 112–120.
[14] G. Tang, X.u. Zhao, R. Li, Y. Liang, Y. Jiang, H. Chen, The effect of arc position on laser-arc hybrid welding of 12-mm-thick high strength bainitic steel, Opt. Laser Technol. 121 (2020) 105780, https://doi.org/10.1016/j.optlastec.2019.105780.
[15] A. Artinov, N. Bakir, M. Bachmann, A. Gumenyuk, M. Rethmeier, Weld pool shape observation in high power laser beam welding, Procedia CIRP 74 (2018) 683–686.
[16] F. Farrokhi, B. Endelt, M. Kristiansen, A numerical model for full and partial penetration hybrid laser welding of thick-section steels, Opt. Laser Technol. 111 (2019) 671–686.
[17] G. Xu, L. Li, H. Wang, P. Li, Q. Guo, Q. Hu, B. Du, Simulation and experimental studies of keyhole induced porosity in laser-MIG hybrid fillet welding of aluminum alloy in the horizontal position, Opt. Laser Technol. 119 (2019) 105667, https://doi.org/10.1016/j.optlastec.2019.105667.
[18] A. Hammad, C. Churiaque, J.M. Sánchez-Amaya, Y. Abdel-Nasser, Experimental and numerical investigation of hybrid laser arc welding process and the influence of welding sequence on the manufacture of stiffened flat panels, J. Manuf. Process. 61 (2021) 527–538.
[19] I. Bunaziv, C. Dørum, X. Ren, M. Eriksson, O.M. Akselsen, Application of LBW and LAHW for fillet welds of 12 and 15 mm structural Steel. NOLAMP17, Proc. Manuf.. 36 (2019) 121–130.
[20] S.E. Webster, Y. Tkach, P. Langenberg, A. Nonn, P. Kucharcyzk, J.K. Kristensen, P. Courtade, L. Debin, D. Petring. Hyblas: economical and safe laser hybrid welding of structural steel: contract no RFSR-CT-2003-00010, 1 September 2003 to 30 June 2007; final report, Corus UK Limited, South Yorkshire, UK, 2009.
[21] C.H.J. Gerritsen, J. Weldingh, J.K. Kristensen, Development of Nd: Yag Laser-MAG hybrid welding of T joints for shipbuilding. Proc. NOLAMP10, 2005.
[22] A. Unt, I. Poutiainen, S. Grünenwald, M. Sokolov, A. Salminen, High Power Fiber Laser Welding of Single Sided T-Joint on Shipbuilding Steel with Different Processing Setups, Appl. Sci. 7 (12) (2017) 1276, https://doi.org/10.3390/app7121276.
[23] I.N. Udin, A.A. Voropaev, A. Unt, Application Development for the Evaluation of Penetration in Laser and Laser-Arc Hybrid Welding of Tee and Corner Joints, Key Eng. Mater. ISSN: 1662-9795 822 (2018) 381–388.
[24] I.A. Tsibulskiy, A.D. Akhmetov, R.S. Korsmik, A.A. Voropaev, R.V. Mendagaliyev, A.D. Eremeev, The influence of the gap size on the formation of a welded joint in hybrid laser-arc welding of angular joints and T-joints, Beam Tech. Laser Appl. IOP Conf. Series: J. Phy.: Conf. Series 1109 (2018) 012033.
[25] ISO 6947:2019, International Organization for Standardization 6947:2019, Welding and allied processes - Welding positions.
[26] American Welding Society (AWS) A3.0M/A3.0:2010, Standard Welding Terms and Definitions.
[27] M. Mazar Atabaki, N. Yazdian, R. Kovacevic, Hybrid laser/arc welding of thick high-strength steel in different configurations, Adv. Manuf. 6 (2) (2018) 176–188.
[28] A. Unt, E. Lappalainen, A. Salminen, Comparison of Welding Processes in Welding of Fillet Joints, Isope 9 (2013) 181–188.
[29] I. Bunaziv, S. Wenner, X. Ren, J. Frostevarg, A.F.H. Kaplan, O.M. Akselsen, Filler metal distribution and processing stability in laser-arc hybrid welding of thick HSLA steel, J. Manuf. Process. 54 (2020) 228–239.
[30] A. Unt, E. Lappalainen, A. Salminen, Autogeneous laser and hybrid laser arc welding of T-joint low alloy steel with fiber laser systems, Phys. Procedia 41 (2013) 140–143.
[31] Bureau Veritas BV NR 216 DT R10 E, Rules on Materials and Welding for the Classification of Marine Units. Chapter 5 - Welding. Section 4 - Approval of Welding Procedures. 2 - Welding procedure qualification tests for C and C-Mn steels for ship hull and other welded structures in general. 2.2. - T butt joints in plates, 2018.
[32] Lloyd's Register, Rules for the Manufacture, Testing and Certification of Materials, July 2017. Chapter 12. Welding Qualifications. Section 2. Welding procedure qualification tests for steels, 2017.
[33] L.F. Scalet Rossini, R.A. Valenzuela Reyes, J.E. Spinelli, Double-wire tandem GMAW welding process of HSLA50 steel, J. Manuf. Process. 45 (2019) 227–233.
[34] F.C. Campbell, Elements of Metallurgy and Engineering Alloys, ASM International, Materials Park, Ohio, USA, 2008, pp. 371–393 (Chapter 20).
[35] ISO 12932: 2013, Welding — Laser-arc hybrid welding of steels, nickel and nickel alloys — Quality levels for imperfections, June, 2013.
[36] E.A. Valdaytseva, I.N. Udin, Determination of the heat source parameters for the case of simultaneous two-sided laser-arc welding of extended T-joints, Beam Tech. Laser Appl. IOP Publ. IOP Conf. Series: J. Phy.: Conf. Series 1109 (2018) 012009.
[37] ISO 15614-14:2013, International Organization for Standardization 15614-14: 2013. Specification and qualification of welding procedures for metallic materials. Welding procedure test. Part 14: Laser-arc hybrid welding of steels, nickel and nickel alloys.